MICROWAVE RESEARCH

Semiannual Status Report No. 2

1 December 1969 – 31 May 1970

for

Office of Naval Research

Con⁺ ˉact N00014-67-A-0112-0039

Project NR 373-361

Code 427

M. L. Report No. 1877

June 1970

Reproduction, in whole or in part, is permitted
for any purpose of the United States Government

Microwave Laboratory
W. W. Hansen Laboratories of Physics
Stanford University
Stanford, California

INTRODUCTION

This report is the Second Semiannual Status Report under Contract N00014-67-A-0112-0039, which began on 1 June 1969.

We continue to start new projects under this program which we feel have potential for developing into major new technical areas, capable of generating separate support based on initial results demonstrated under the Joint Service Program. The preceding report discussed three project areas originated under the Joint Service Program which had attained that status, and were being continued and appreciably expanded under new auspices, namely the acoustic surface wave amplifier, the acoustic microscope, and an ultraviolet laser project. These have grown into separate contracts of real significance. The surface wave amplifier provides very large stable gain over wide bandwidth and is moving closer to incorporation for overcoming losses in practical delay lines for signal processing. Industrial development for this purpose is underway. Acoustic microscope components of both direct imaging and scanning types, both of which originated under the Joint Service Program, are showing behavior in accordance with expectations, and initial testing with biological specimens is beginning under the follow-on program.

During the reporting period a new area of vacuum deposition of semiconductor films for UHF and microwave device work has been added to the Joint Service Program. This work was inspired by promising findings under the follow-on surface wave amplifier contract referred to above, that indium antimonide can be vacuum deposited having a new range of dc parameters suitable for use with the surface wave amplifier, and that semiconductor fabrication for the amplifier could be tremendously simplified by vacuum deposition techniques if the rf parameters of the films could also be brought into the correct range. This is a speculative idea with

large prospective payoff in device cost and performance. It has been possible during the few months that it has been active under the Joint Service Program to obtain promising results in pinpointing the rf parameters which are relevant in semiconductor films for high frequency devices, and in making progress toward the achievement of these parameters. Other materials are also to be tried, and there is the possibility that general vacuum deposition of semiconductors will grow into a major activity in this laboratory.

During the reporting period we have undertaken development of a general computer program for calculating acoustic propagation in systems consisting of a thin film on a substrate, which includes as special cases all problems of surface wave propagation on a single surface, guided wave and dispersive wave propagation in thin layers on a substrate, and general focusing and deflection of surface type waves. Until recently it has been possible to use simple programs which assumed the materials are isotropic and nonpiezoelectric, but current experimental device work with strongly anisotropic and piezoelectric materials required that both these characteristics be included, and both of them necessitate major programming steps. The program is now in operation with arbitrary anisotropy in both the substrate and film and the addition of arbitrary piezoelectricity is underway; it is finding essential application to a variety of surface wave device projects within the laboratory.

A third new program which was added at the beginning of the reporting period is a theoretical and experimental investigation of parametric amplification of surface acoustic waves as a possible means for low noise amplification in surface wave delay line devices and for the generation of surface waves at UHF and microwave frequencies. A new parametric interaction between acoustic and electrical waves in piezoelectric crystals is involved which was first discovered in bulk wave delay lines on another program in this laboratory. While bulk waves have high dynamic range which makes

them essential in some applications, they also require high
threshold power for parametric oscillation.

It was predicted that surface waves would be capable of low
thresholds and this question is now being investigated under the
current program.

It will be noted in the text that some current projects are
nearing completion and this circumstance will be accompanied by
the addition of further new research areas under the program.   At
the present time, six projects are active under this contract.

    I.   Theory of Thin Film Waveguides

   II.   Tunable Raman Laser

  III.   Ring Lasers

   IV.   Surface Wave Parametric Amplification

    V.   Semiconductor Films

   VI.   Submillimeter Wave Generator

In the text below, certain introductory parts of the project reports
are repeated each time so the reader may more readily follow the
work without reference to previous reports.

The responsible investigator is M. Chodorow; C.F. Quate is co-
responsible investigator.

TABLE OF CONTENTS

Preceding page blank

LIST OF FIGURES

I.   THEORY OF THIN FILM WAVEGUIDES

(B. A. Auld, L. P. Solie, and H. J. Shaw)

During the past reporting period we have developed a computer
program capable of finding the dispersion relations for guided acoustic
waves in a film supported by a semi-infinite substrate where both mate-
rials are nonpiezoelectric but otherwise arbitrarily anisotropic. The
mathematical approach is essentially the same as was described in the
previous reporting period for the anisotropic free plate so no detailed
theoretical derivation is necessary. A guided wave is composed of a
sum of solutions which individually must satisfy the equation of motion
in their respective media; the sum of these solutions must satisfy the
following boundary conditions: 1) zero normal stress at the free surface
of the film, 2) continuous normal stress across the boundary between the
film and substrate, 3) continuous displacement vector across this same
boundary, and 4) displacement vector components must vanish exponentially
into the substrate.

A typical dispersion curve is shown in Fig. 1 when phase velocity
is plotted versus the product of film thickness h and wave number k
for a gold film on sapphire. The gold film, though nearly isotropic,
is oriented with a cubic axis normal to the surface and another cubic
axis in the direction of propagation. The sapphire is X cut Y pro-
pagating.

A second program developed during this reporting period was a
special case of the above program. This program calculated the surface
velocity for an arbitrarily oriented anisotropic surface wave with no
film present. These waves are nondispersive but depend upon crystal
orientation with respect to the surface normal and the direction of
propagation as shown for $LiNbO_3$ in Fig. 2. For this figure the Y and
Z crystal axes lie in the plane defined by the surface normal and the
propagation direction. The angle between the surface normal and the
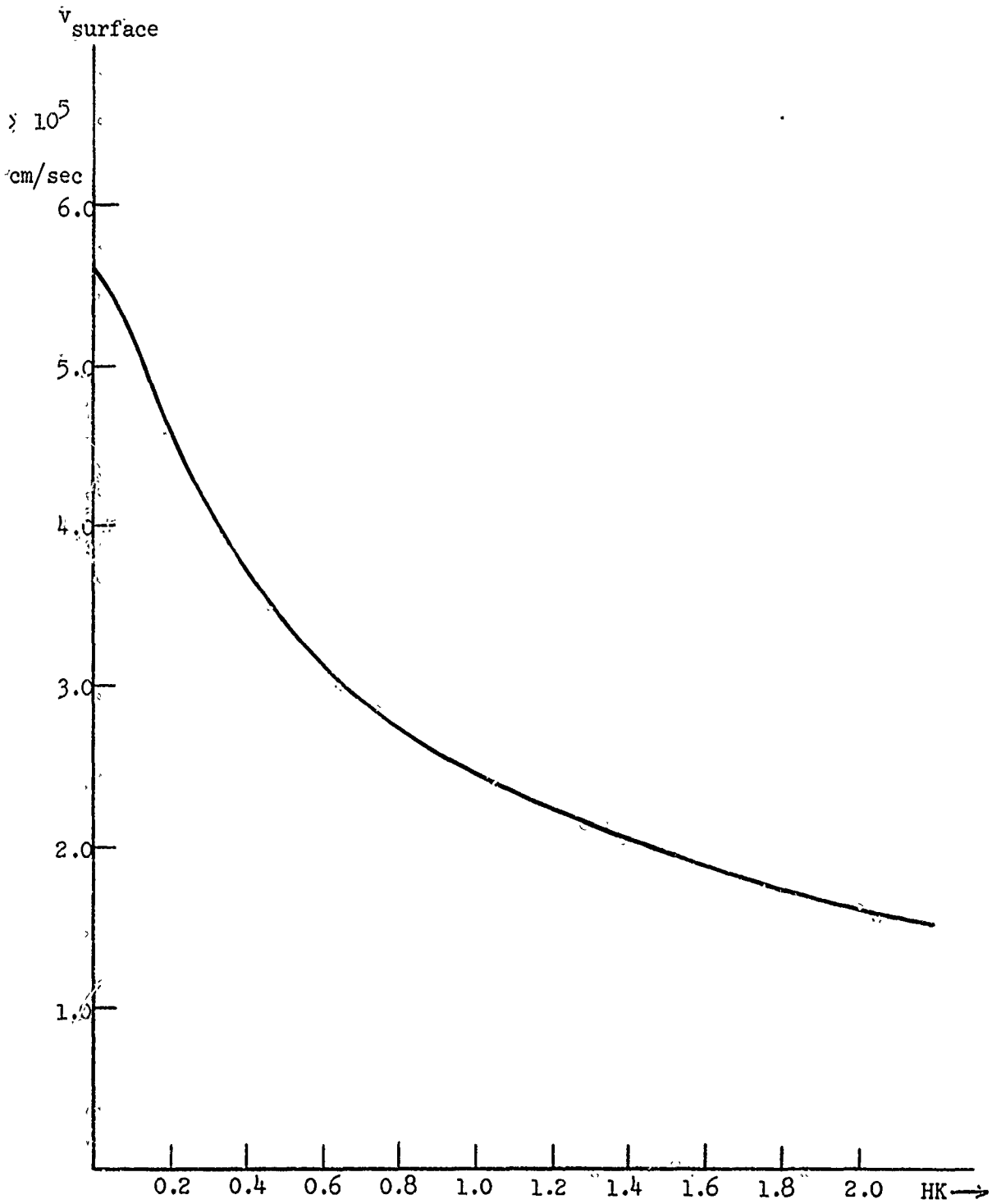Z axis is θ ; velocity is in cm/sec divided by 10^5. As indicated

FIG. 1--Velocity versus film thickness-wavenumber for the lowest order
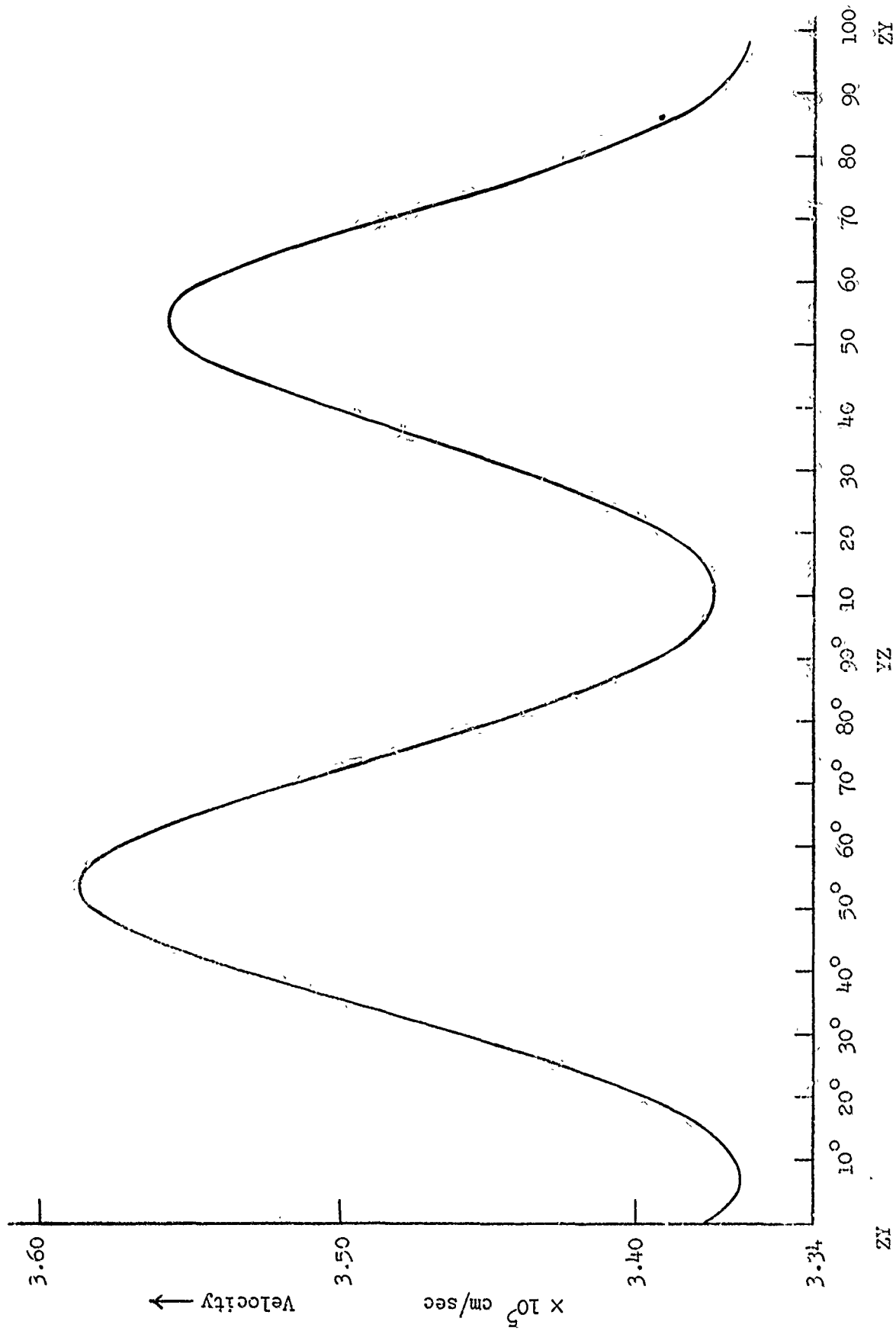surface wave for gold on sapphire.

FIG. 2--Surface wave velocity versus angle for LiNbO$_3$.

in the figure, $\theta = 0^\circ$ and 180° corresponds to Z cut, x propagating while $\theta = 90^\circ$ is Y cut, Z propagating.

The latter part of this reporting period was devoted to extending these analyses to include piezoelectric effects. Using the quasistatic approximation for the electric field, the following is the equation of motion for acoustic waves in a piezoelectric medium.

$$\left(\overleftrightarrow{1} : \left\{ \overleftrightarrow{c}^E + \frac{(\overleftrightarrow{e} \cdot \vec{\ell})(\vec{\ell} \cdot \overleftrightarrow{e})}{\vec{\ell} \cdot \overleftrightarrow{\epsilon}^S \cdot \vec{\ell}} \right\} : \nabla_s - i\rho V^2 k_1 \right) \vec{u} = 0 \qquad (1)$$

where $\vec{k}$ is the propagation vector

$$\vec{\ell} = \frac{\vec{k}}{k_1}$$

V = the surface wave velocity

ρ = the mass density

$\overleftrightarrow{c}^E$ = the stiffness constants

$\overleftrightarrow{\epsilon}^S$ = the dielectric constants

$\overleftrightarrow{e}$ = the piezoelectric constants

$\vec{u}$ = the displacement vector.

Solutions to this equation are sought in the form

$$u_i = \alpha_i e^{ik_1(\ell_1 X_1 + \ell_3 X_3 - Vt)} , \qquad (2)$$

where the surface wave propagates along X_1 and X_3 is normal to the surface. Here, α_i are constants describing the phase and amplitude relationship between the components of u_i for a given solution. In order for solutions α_i to exist, the secular determinant of Eq. (1)

- 4 -

must vanish. The resulting equation is an eighth order polynomial in l_3 when the coefficients are functions of the velocity v. Considerable effort has been made to express these coefficients as explicit functions of v in order to make the calculation of the l_3's as efficient as possible since, in the numerical calculations, this operation is repeated many times in a reiterative loop. This step has recently been finished and the next step is to impose boundary conditions for various guided mode problems.

must vanish. The resulting equation is an eighth order polynomial in l_3 when the coefficients are functions of the velocity v. Considerable effort has been made to express these coefficients as explicit functions of v in order to make the calculation of the l_3's as efficient as possible since, in the numerical calculations, this iteration is repeated many times in a roiterative loop. This step has recently been finished and the next step is to impose boundary conditions for various guided mode problems.

II.   TUNABLE (IR) RAMAN LASER

(R.H. Pantell, H.E. Puthoff, S.S. Sussman, B.C. Johnson, and J. SooHoo)

A.   INTRODUCTION

The purposes of this investigation are to study the conversion of energy from one frequency to another utilizing the Raman effect; to develop continuously-tunable optical and far-infrared sources with desirable spectral and coherence properties; and to obtain a clear understanding of the materials and mechanisms involved in this non-linear process.

B.   MAJOR ACCOMPLISHMENTS

1.   Experimental Work

A simple, highly-efficient, tunable infrared and optical source has been developed. In the infrared the radiation can be tuned continuously from 50 to 250 microns with powers of 10 to 100 watts. In the visible the source can be tuned over 100 angstroms with a conversion efficiency from a 1-megawatt ruby laser pump of greater than 50%. The device consists simply of a lithium niobate ($LiNbO_3$) crystal placed in front of a Q-switched ruby laser. Tuning is achieved by rotating the crystal so that the angle between the pump beam and the normal to the crystal faces is varied. External resonators are not required, and the device operates at room temperature, eliminating the need for crystal temperature control.

We have recently measured the power versus wavelength characteristics for the infrared signal output. The results agree with theory. Peak powers of ~ 150 watts at 200 microns are generated with no crystal damage as a typical result. In addition line-width measurements have been completed which indicate bandwidths of ~ 1.5 m^{-1} for the radiation over the observed tuning range of 50-200 microns. These results are presented in the Appendix.

2. Theoretical Work

In the stimulated Raman process of interest, energy intensity at the pump frequency is converted into energy intensities at both the shifted Raman (visible) frequency and the infrared frequency. Hitherto, in theoretical analyses of the problem depletion of the pump intensity as a result of conversion to other frequencies has been neglected. Due to the efficiency of the process (i.e., observed high conversion) we have begun to investigate the effects of pump depletion. Closed-form solutions have been obtained. Computations and experimental verification of the theoretical predictions are now underway.

3. Further Work

As a result of the success of the project, other crystals to provide further extension of the work are being investigated, both theoretically for their properties and experimentally by being grown in the crystal research laboratory. If anticipated results are forthcoming, it will be possible to extend the results obtained thus far to new frequencies and also to cw operation.

APPENDIX

II.   TUNABLE RAMAN LASER

POWER AND LINEWIDTH OF TUNABLE STIMULATED FAR IR EMISSION

IN LiNbO$_3$[*]

B. C. Johnson, H. E. Puthoff, J. SooHoo, and S. S. Sussman

Stanford University
Stanford, California 94305

ABSTRACT

The power versus wavelength characteristic for a high power, continuously tunable far infrared source has been experimentally determined and compared with theory. Utilizing a Q-switched ruby laser as the pump and stimulated polariton scattering in the crystal LiNbO$_3$ as the scattering mechanism, peak powers of $\sim$ 150 W at 200 microns are generated without crystal damage. Linewidth measurements indicate a bandwidth of < 0.5 cm^{-1} for the radiation over the observed tuning range of 66 to 200 microns.

We recently reported the direct detection of tunable stimulated far infrared radiation accompanying optical scattering from the lowest A_1 -symmetry polariton mode in LiNbO$_3$.[1,2] The stimulated radiation results from a parametric process whereby input pump photons of frequency ν_p interact with an optical vibrational mode in the crystal at frequency ν_i , producing "signal" radiation at $\nu_s = \nu_p - \nu_i$ and "idler" radiation at ν_i . Since the idler frequency and wave vector must lie on the material dispersion characteristic (ω - k diagram), a unique set of allowed frequencies and wave vectors is determined for the scattering process.[3] Simultaneous tuning of signal and idler is then accomplished by varying the angle between pump and signal propagation vectors.

In our experiment, opposite ends of an uncoated a-axis LiNbO$_3$ crystal were polished flat and parallel to form a low Q resonator or the signal radiation. Tuning was accomplished at room temperature by mechanically varying the angle between the pump beam and the crystal surface normal. The pump, signal, and idler are linearly polarized parallel to the crystal c-axis.

The experimental arrangement is shown in Fig. 1. The pump was a Q-switched ruby laser (6943 Å) emitting 20 nsec. pulses with a peak power of ~ MW and a beam diameter at the laser of about 2 mm. A 50 cm focal length lens focused the beam near the output end of a 3.- cm a-axis LiNbO$_3$ crystal with the laser polarized along the c-axis. The laser-lens combination is mounted on a rotatable bench with its pivot point coinciding with the output end of the crystal, which rests

on a fixed platform. The end faces of the crystal were polished flat and parallel to within a few seconds of arc. In addition, a cut was made in the corner of the crystal output end at the proper angle to allow the idler radiation to emerge approximately normal to the exit surface and hence minimize reflection loss at the crystal-air interface. IR detection was provided by a calibrated Golay detector system, with a black polyethelyne filter placed in the collecting light pipe to eliminate stray optical signals. Outputs from this detector were monitored on a Tektronix Type 555 oscilloscope. Temporal behavior of input pump, output pump, and signal radiation was monitored on photo-diodes in conjunction with a Tektronix Type 519 oscilloscope. Optical wavelengths are recorded on film at the output of a 1 M grating spectrometer. Measurements of the signal radiation linewidth were performed with a Fabry-Perot interferometer. The transmitted output pump beam was blocked during the linewidth measurements.

Figure 2 shows the observed tuning curve for the crystal use n the experiment. The signal and idler radiation was monitored di ctly for each of the points indicated on the figure. Detailed behavior of the frequency tuning as the angle of incidence is varied, has been treated elsewhere.[1,4]

The magnitude and frequency dependence of the scattered idler power may be estimated theoretically. Proceeding from rate equations, we obtain that power at the idler frequency, P_i , generated inside the crystal is given by

$$P_i = \frac{\nu_i}{\nu_s} \left(\frac{g_s \cos \phi}{g_s \cos \phi + \alpha_i} \right) P_s , \qquad (1)$$

- 10 -

where g_s , the signal gain constant, satisfies the growth equation

$$\frac{\partial P_s}{\partial z} = g_s P_s \quad ,$$

ϕ is the angle between pump and idler propagation vectors (see Fig. 1), and α_i is the idler absorption constant. The value of α_i is determined from infrared reflectivity data,[6] and all other parameters in Eq. (1) can be evaluated from a plane wave treatment of the scattering process.[7] The resulting theoretical curve r normalized idler power versus wavelength appears as the solid line on Fig. 3, for which we have assumed a ruby pump with an intensity of 5×10^8 W/cm^2, the approximate value used in the experiment. For a signal power $P_s \sim 10^6$ W (corresponding to experimentally observed values), Fig. 3 implies a peak idler power $P_1 \approx 150$ W generated inside the crystal at $v_i = 50$ cm^{-1} ($\lambda_i = 200 \mu$). Experimental points appear as dots on the figure with accuracy indicated by error bars. The measured idler power outside the crystal is reduced from the plotted internally generated power by a factor of about twenty, primarily due to surface reflection and absorption between the generating volume and the exit face.

We may quantitatively determine some additional characteristics of the idler radiation based on a knowledge of the signal frequency bandwidth. Conservation of energy for the scattering process requires that $\Delta v_i \leq \Delta v_s$, where $\Delta v_{i,s}$ refer respectively to the idler and signal linewidths. Fabry-Perot measurements performed on the signal radiation over the observed tuning range indicated values for Δv_s ranging from

about 0.1 to 0.5 cm^{-1}. Hence we infer that the idler radiation in our experiment exhibited a linewidth, Δv_i , of less than 0.5 cm^{-1} throughout the tuning range.

Having determined the linewidth of the idler radiation, it then becomes possible to estimate its spatial divergence. The material dispersion curve[1,6] indicates, for a given frequency interval Δv_i along the curve, a corresponding wave vector spread Δk_i for the idler radiation. Since the idler wave vector determines its propagation direction, a Δk_i results in spatial spreading of the idler output beam. Thus by knowing Δv_i , we may estimate the angular divergence of the radiation as it emerges from the crystal exit face. For a Δv_i of ~ 0.5 cm^{-1} the average value for the angular divergence outside the crystal is approximately 2.5 degrees.

In summary, power and linewidth measurements have been accomplished for a stimulated coherent far infrared source, tunable from 66 to 200 microns. High peak power (~ 1.0 W), narrow frequency linewidth, and small angular divergence characterize the output radiation, which was directly detected over the entire tuning range. Some interesting features of the source are its simplicity, continuous tunability, and room temperature operation.

REFERENCES

1. J.M. Yarborough, S.S. Sussman, H.E. Puthoff, R.H. Pantell, and B.C. Johnson, Appl. Phys. Letters 15, 102 (1969).

2. S.S. Sussman, B.C. Johnson, J.M. Yarborough, H.E. Puthoff, R.H. Pantell, and J. SooHoo, Submillimeter Waves (Polytechnic Institute of Brooklyn, Microwave Research Institute, Symposium XX), to be published.

3. H.E. Puthoff, R.H. Pantell, B.G. Huth, and M.A. Chacon, J. Appl. Phys. 39, 2144 (1968).

4. J.M. Yarborough, Microwave Laboratory Report No. 1816, W.W. Hansen Laboratories of Physics, Stanford University, Stanford, California (1969).

5. C.H. Henry and C.G.B. Garrett, Phys. Rev. 171, 1058 (1968).

6. A.S. Barker, Jr. and R. Loudon, Phys. Rev. 158, 443 (1967).

7. S.S. Sussman, Microwave Laboratory Report No. 1851, W.W. Hansen Laboratories of Physics, Stanford University, Stanford, California (1970).

FIGURE CAPTIONS

1. Schematic diagram of the experimental setup. Idler radiation emerges approximately normal to corner face of $LiNbO_3$ crystal and is monitored by Golay detector-light pipe combination. L is a 50 cm focal length lens, BS denotes beam splitters, PD1 and PD2 are photodiodes, and D indicates diffusers used to uniformly illuminate spectrometer slits. Pump, signal and idler propagation directions and angles are indicated by phase matching triangle at upper left. Rotation of laser bench varies θ', and hence θ .

2. Observed tuning curve. Scale at left represents idler frequency ν_i in wave numbers, scale at right the corresponding wavelength $(1/\nu_i)$.

3. Normalized idler power versus wavelength generated inside crystal. Theoretical analysis indicated by solid curve with dots corresponding to experimentally observed points. Idler frequency and wavelength indicated on bottom scales. Idler power outside the crystal is reduced by a factor of about 20 due to surface reflection and absorption between the generating volume and the exit face.
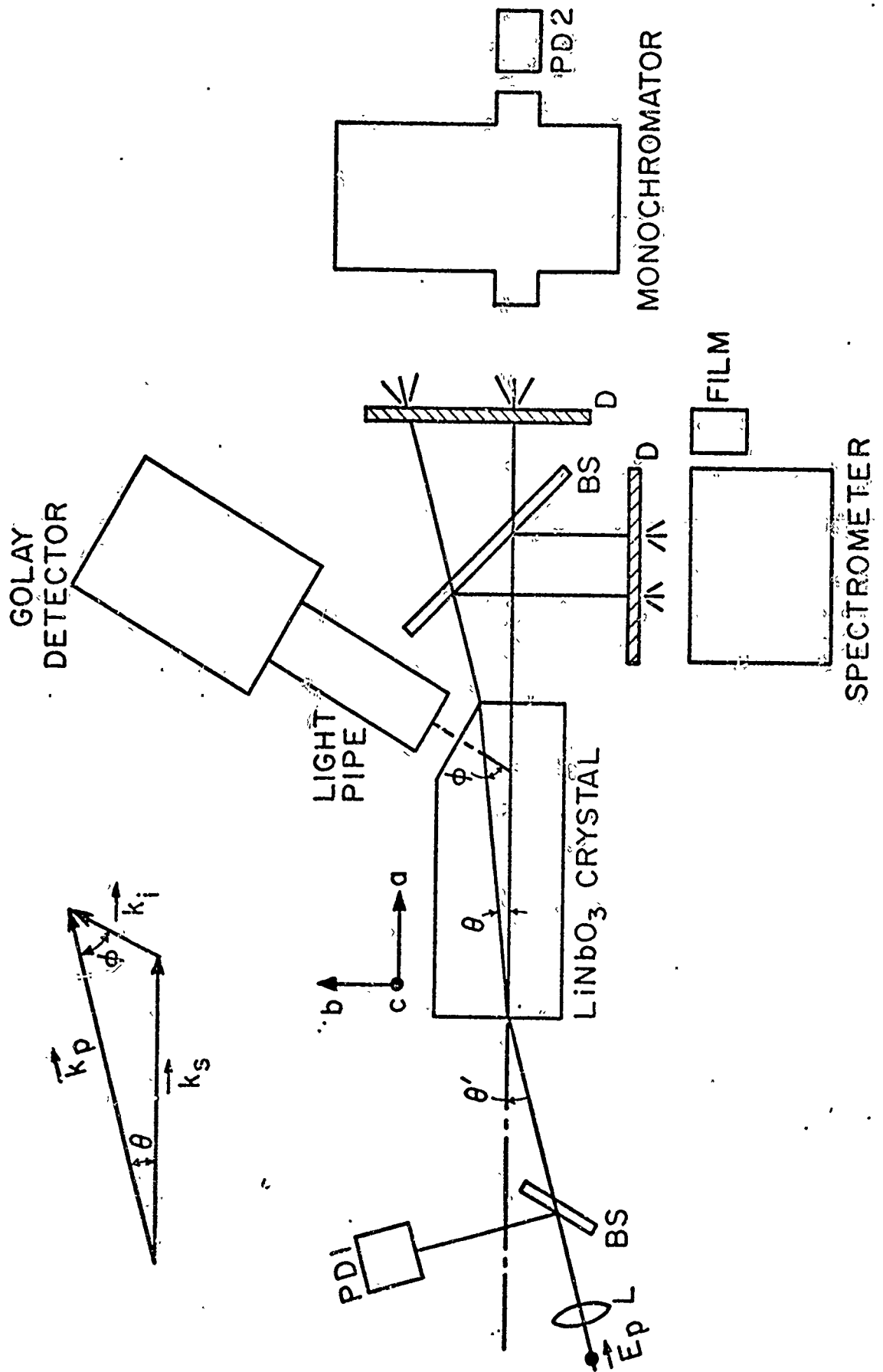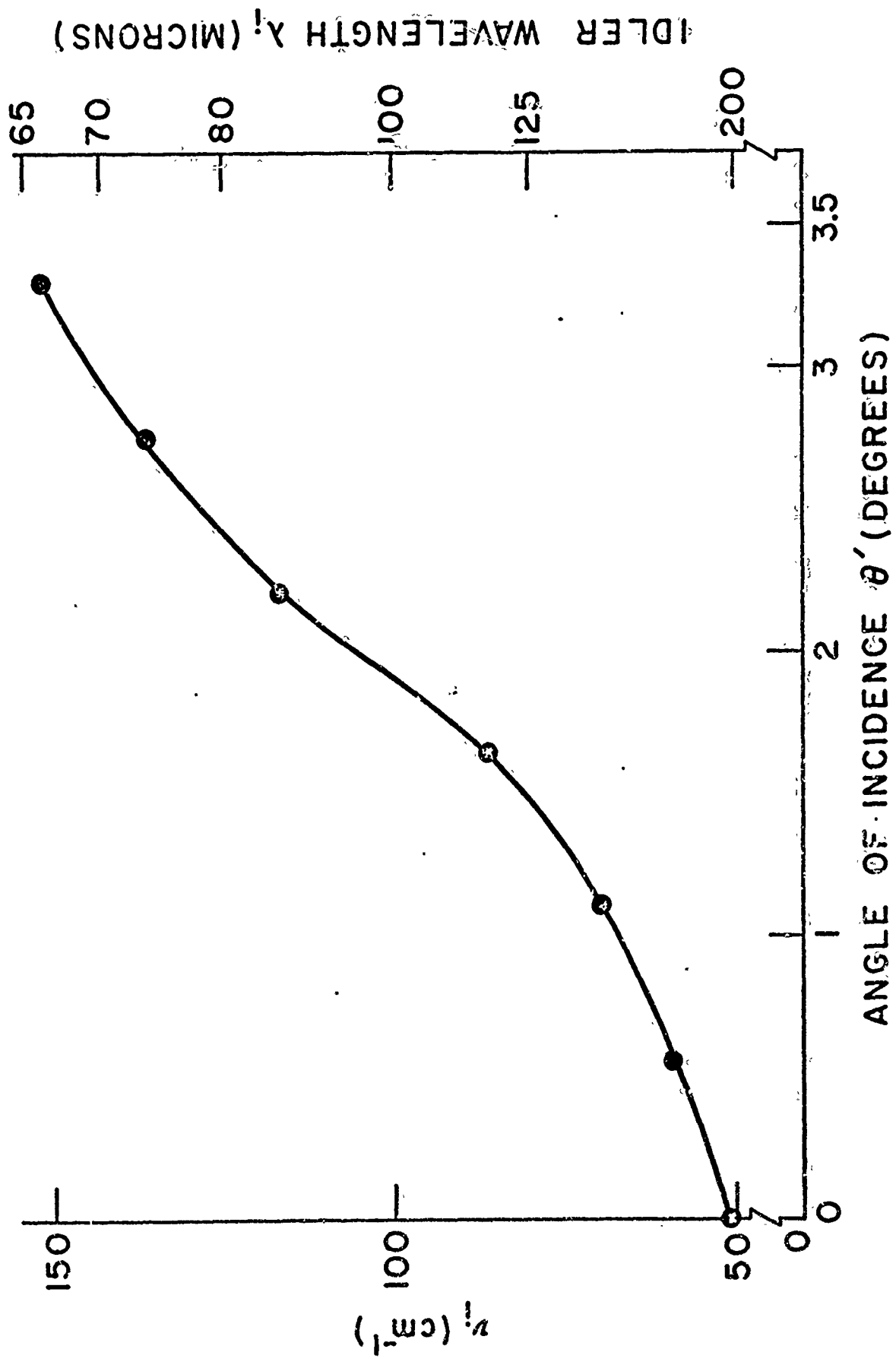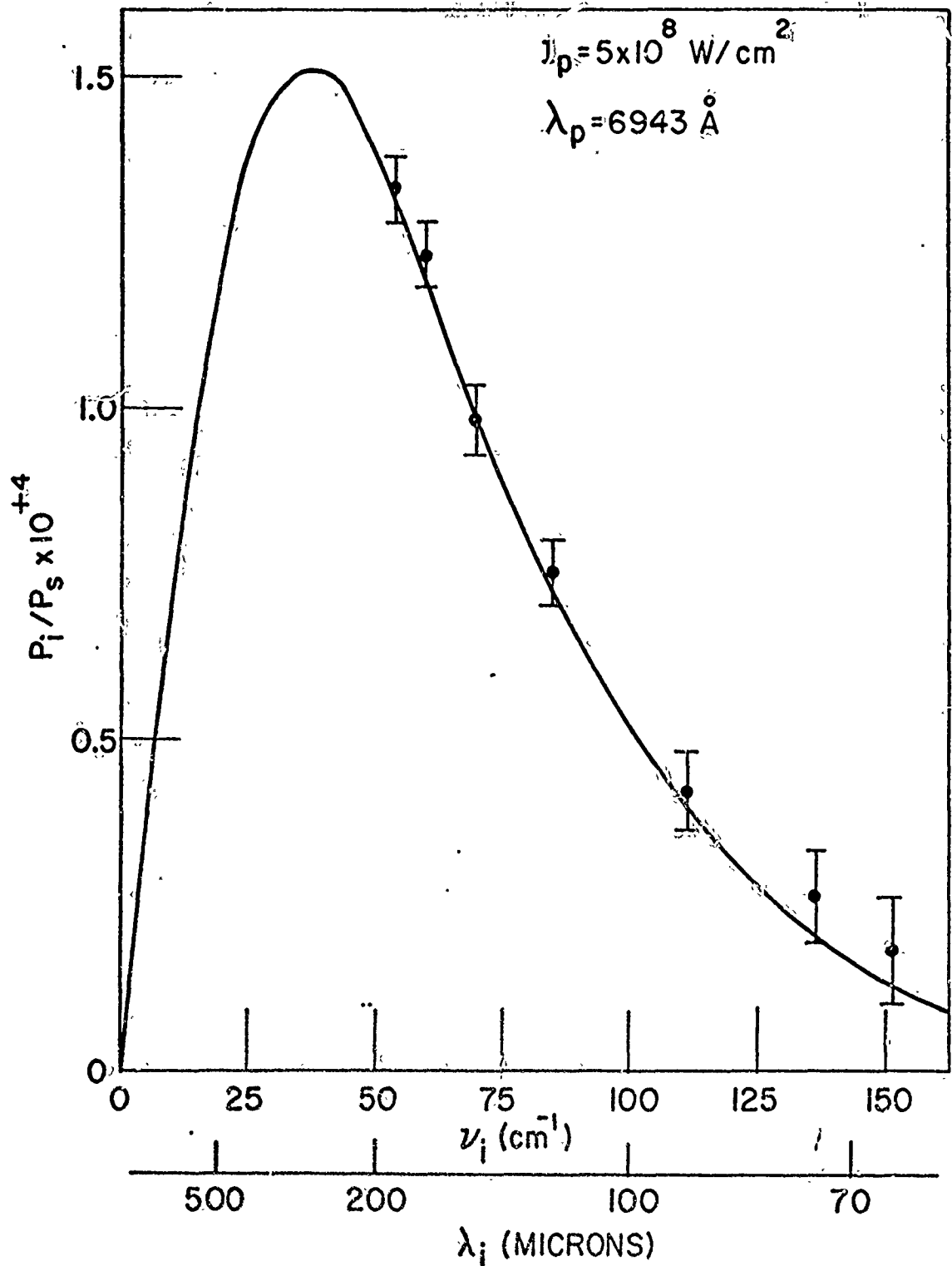
FIGURE 1

FIGURE 2

IDLER WAVELENGTH λ_i (MICRONS)

ANGLE OF INCIDENCE θ' (DEGREES)

ν_i (cm^{-1})

- i -

FIGURE 3

III. RING LASERS

(M. Chodorow, H. E. Puthoff, S. I. Wax)

A. INTRODUCTION

In this project we are studying the effect of frequency modulation on the behavior of a ring laser. The goals are to develop techniques which might be used to improve the low frequency sensitivity of a ring laser, and to better understand the physical phenomena involved in the operation of the device.

Previous research, sponsored by the Air Force under contract AF 33(615-67-C)1245, dealt with the behavior of the ring laser in the presence of pulses produced by intracavity phase modulation. A report on that research is given in Appendix A.

B. EXPERIMENTAL RESULTS

Research on this contract has dealt with the condition of frequency modulation. As described in Appendix A, this condition may be achieved by detuning the phase modulator about 300 MHz away from mode spacing.

In order to monitor the frequency modulated optical spectrum, a confocal-cavity scanning interferometer has been constructed. Using this device we have been able to verify the presence of a single frequency-modulated spectrum, whose modulation index varies in the range between about 5 and 10 as we vary the modulator frequency and depth.

Measuring the beat between oppositely directed waves, we found a frequency offset in absence of rotation. The offset is of the order 1-2 kHz, and thermally drifts over several hundred Hz. Besides being deleterious to rotation sensing, this result is at first surprising. In the pulsed case we attributed the offset to the localization of energy so that a pulse arrives at the modulator at a particular time. However, in the FM case, the intensity is uniform and we may not speak of an arrival time. The offset in this case comes from mode pulling resulting from the large modulator detuning. A slight difference

between the spectral shapes of the oppositely-directed waves causes a
difference in net mode pulling and thus an offset. The drift in offset
results from the extreme sensitivity of relative mode amplitudes to
the parameters of the system.

In the FM case, as in the pulsed case, we note the existence of
two states, analogous to the 0 and II pulse states (described in
Appendix A). The offset changes as we switch between the two FM states,
and in one state locking never occurs, while in the other there is
locking with hysteresis. This behavior is not understood, and in fact
it is not clear whether the theory predicts the existence of two FM
states. Some further effort will be made to understand this behavior.

between the spectral shapes of the oppositely-directed waves causes a
difference in net mode pulling and thus an offset. The drift in offset
results from the extreme sensitivity of relative mode amplitudes to
the parameters of the system.

In the FM case, as in the pulsed case, we note the existence of
two states, analogous to the O and II pulse states (described in
Appendix A). The offset changes as we switch between the two FM states,
and in one state locking never occurs, while in the other there is
locking with hysteresis. This behavior is not understood, and in fact
it is not clear whether the theory predicts the existence of two FM
states. Some further effort will be made to understand this behavior.

APPENDIX A

III. RING LASER PROJECT

Research directed by
Professor Chodorow

1. INTRODUCTION

This project is concerned with research on the properties of an electromagnetic rotation sensor, more commonly referred to as a ring laser. In particular, it is concerned with approaches which can probably overcome the principal disadvantages of existing ring lasers.

A ring laser is an optical oscillator with mirrors placed at the corners of a polygon. The light follows the closed path around the perimeter, so that the natural modes will consist of running waves, traveling in opposite directions around the ring. The resonant condition is that the round-trip pathlength be an integral number of wavelengths. In the presence of rotation, general relativity tells us that the pathlengths for light traveling in opposite directions will be different so that the frequencies of the oppositely-directed (OD) waves are different by an amount

$$\Delta f = \frac{4A}{\lambda P} \Omega$$

where

Δf = frequency difference between OD waves in cycles/sec

A = area of the polygon normal to the axis of rotation

λ = optical wavelength

P = perimeter of the polygon

Ω = rate of rotation in radians/sec

Thus, we may use the beat frequency between oppositely-directed waves as a linear measure of absolute rotation rate.

The use of the **ring laser as a rotation-rate** sensor has, in the
past, had **several limitations as the rotation** rate becomes small. A
laser **normally oscillates at several closely** spaced frequencies, or
axial modes. In a **multimode laser,** competition between these axial
modes produces frequency pulling and amplitude jitter causing the out-
put to be incoherent so that low frequency beat notes cannot be meas-
ured. To overcome this effect, it is common to operate ring lasers
under conditions in which only one mode oscillates in each direction,
but this results in a weak and noisy signal. More important, single-
mode operation often produces a frequency error which depends strongly
upon the ring perimeter, varying by kHz's for length changes less than
a wavelength. Thus, very elaborate thermal and mechanical engineering
procedures must be followed to achieve a stable signal. Another diffi-
culty arises as a result of coupling between the oppositely-directed
waves, by mechanisms such as backscattering. Such coupling causes the
oppositely-directed waves to lock together in frequency at low rotation
rates so that the beat signal disappears.

In other laboratories, frequency bias or dithering techniques
have been used to avoid the problem of sensing low rotation rates. In
this laboratory, we are using intracavity modulation techniques in an
attempt to directly improve the sensitivity to low rotation rates,
using all the modes of a multimode laser.

Our modulation techniques overcome both of the limitations ex-
pressed above. The frequency spacing and phase difference between
adjacent axial modes is fixed by the modulator, producing a low-noise
coherent multimode signal. And the waves in opposite directions are
isolated from each other through the production of either narrow pulses
or frequency modulation, reducing the possibility of coupling and
locking.

Two types of modulation have been used in this laboratory.
One method consists of loss modulation in which a time-varying optical
loss produces pulses which arrive at the modulator during the time of
minimum loss. A detailed report on this portion of the project, in

the form of a Ph.D. dissertation, is available [Ref. A-1]. The other method, to which we devote this report, is phase modulation, using an element whose optical length is a function of time. By properly adjusting the modulation drive frequency, it is possible to produce either short pulses or frequency modulation.

## 2. DISCUSSION OF PHASE MODULATION

Intracavity phase modulation of a linear, two-mirror laser is discussed theoretically by Harris and McDuff [Ref. A-2], and experimentally by Amman et al [Ref. A-3]. We have found that a phase perturbation in a ring laser behaves similarly to that in a linear laser. The above references give a rather detailed quantitative prediction of the behavior, but physical insight may be gained by a qualitative discussion.

Consider the lasers shown in Fig. A-1, containing a phaser modulation element within the optical feedback path. The optical length of the modulator varies in time, as shown in Fig. A-2. Thus light passing through the modulator undergoes a Doppler shift in frequency, proportional to the rate of change of optical length. Since the modulator is within the laser feedback path, light passes the modulator many times, and the Doppler shift is regenerative. If the modulation frequency is tuned to the axial mode spacing, i.e., the modulation period equals the optical round-trip time for the cavity, a given point in the light wave arrives at the modulator at the same modulator phase each pass. Thus energy arriving while the length is changing will eventually have its frequency shifted outside the gain bandwidth of the active medium. The light will hence tend to concentrate in pulses which pass through the modulator when its length is stationary. Therefore, there are two distinct pulse trains which can exist in a particular direction: one passing the modulation at 0 modulator phase and one at π .

In the linear laser, or in a particular direction in the ring,

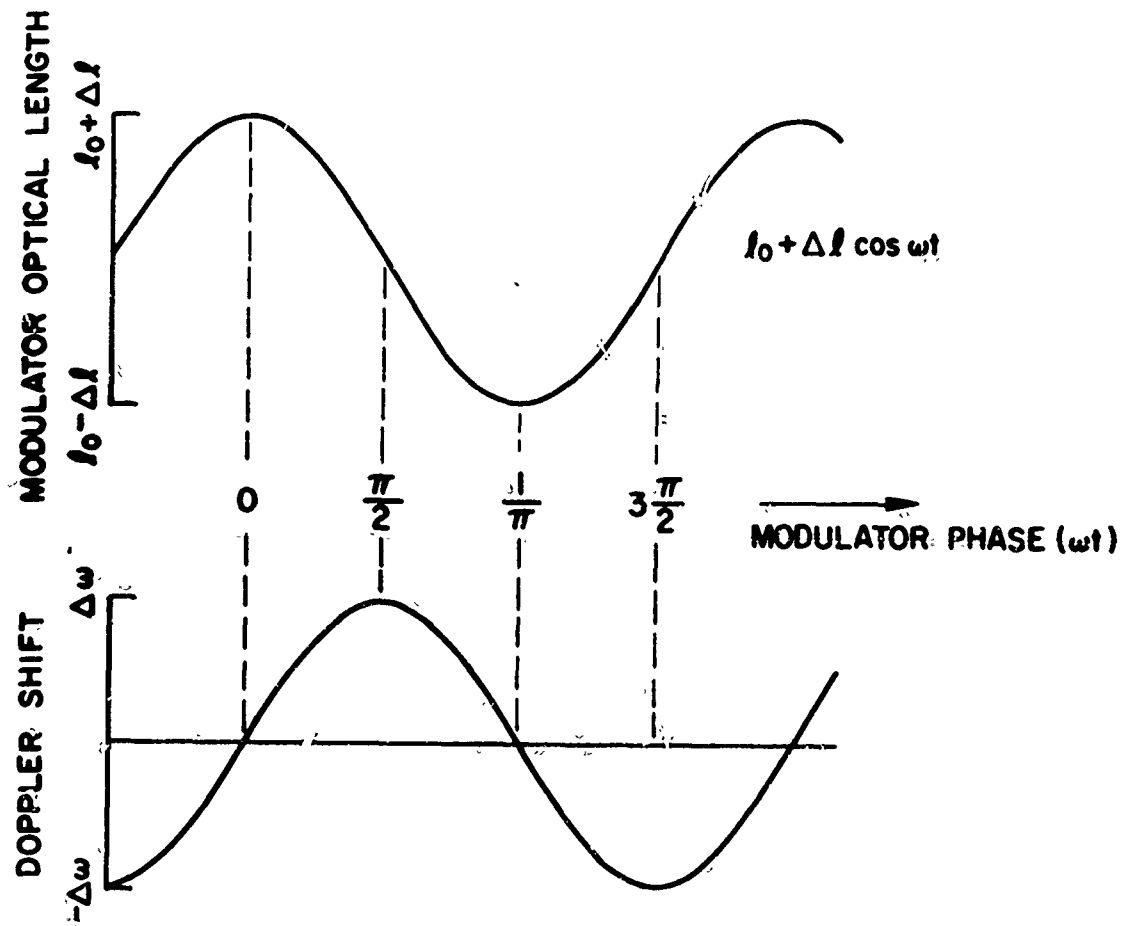ACTIVE MEDIUM   MODULATOR

a. LINEAR LASER

ACTIVE MEDIUM
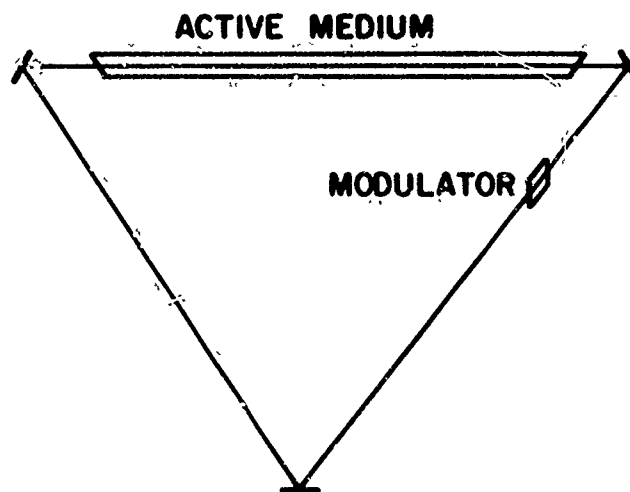
MODULATOR

b. RING LASER

FIG. A-1.   PHASE MODULATION IN LINEAR AND RING LASERS

Light undergoes Doppler shift proportional to change of
length. Maximum shift occurs at $\pi/2$, $3\pi/2$. Light
passing through at 0, π is not shifted.

FIG. A-2. EFFECT OF PHASE MODULATION

we then have four possible results: Both wave trains may exist simul-
taneously, giving two pulses per modulator cycle, a condition we refer
to as double pulses;   one pulse train may be extinguished, leaving a
single pulse per modulator cycle, either at 0 or at π;   or, finally,
both pulse trains may be extinguished.   For a ring laser oscillating
in both directions, there are two possible pulse trains in each di-
rection, with a total of sixteen types of pulsing possible, as enu-
merated in Table 1.   The type of pulsing that results is determined by
coupling between all the pulse trains in the active medium, and is a
function of the modulator tuning and depth.

The position at which oppositely-directed pulses will cross is
determined by both the active medium and the modulatos.   Because of
competition for gain, the active medium prefers the pulses to arrive
such that the delay between successive pulses is maximum.   In the case
of single pulses in both directions, the crossings will be 1/4 of
the ring perimeter from the center of the medium.   We call these points
"natural crossings," and in most of our experiments the modulator is
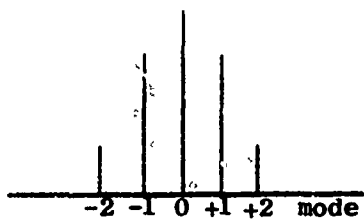placed there.

Returning to Fig. A-2, if the modulator frequency is tuned away
substantially from axial mode spacing, successive Doppler shifts will
still add regeneratively, but not in phase.   The result will be that
each axial mode will have a frequency which varies substantially in
time.   Viewed in the frequency domain (Fig. A-3), each mode has an
f-m spectrum.   These spectra all compete for gain in the active medium,
and the one nearest line center will quench all the others, producing
a single f-m spectrum.

3.   EXPERIMENTAL SETUP

The modulation element used in these phase modulation experiments
is a $45°$ z-cut KDP rod as shown in Fig. A-4.   Note that the ends are
cut at Brewster's angle to reduce backscattering.   To drive the modu-
lator at 75 MHz, a matching circuit was placed in the modulator box
(see Fig. A-5).   Two features of the modulator box are worthy of note:

TABLE A-1. POSSIBLE TYPES OF PULSING FOR PHASE-MODULATED RING LASER

Direction:	Clockwise		Counterclockwise		
Phase:	0	π	0	π	
Type No.					Description
1	X	X	X	X	Doubles in both directions
2	X	X	X	–	
3	X	X	–	X	
4	X	–	X	X	Double and single
5	–	X	X	X	
6	X	X	–	–	
7	–	–	X	X	Double in one direction
8	X	–	X	–	
9	–	X	–	X	Singles cross at modulator
10	X	–	–	X	
11	–	X	X	–	Singles cross away from modulator
12	X	–	–	–	
13	–	X	–	–	
14	–	–	X	–	Single in one direction
15	–	–	–	X	
16	–	–	–	–	Total extinction

X   indicates set of pulses is not extinguished.

Free Running Spectrum

$$-2 \quad -1 \quad 0 \quad +1 \quad +2 \quad \text{mode}$$

Each mode generates its own f-m spectrum.

f-m spectrum of 0th mode

f-m spectrum of 1st mode

f-m spectrum of -1st mode

before inter-action
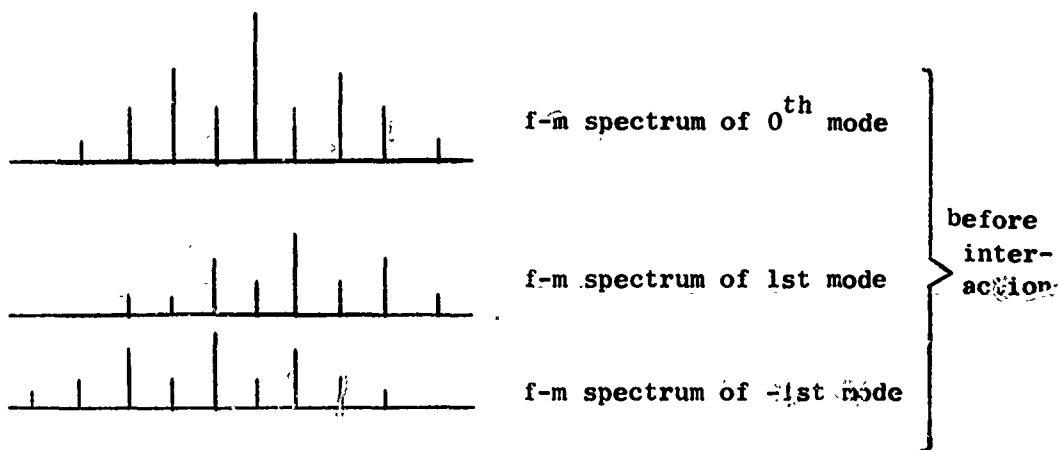
Sidebands of adjacent f-m modes overlap, and thus are coupled together by medium. Spectrum with greatest gain tends to squelch others.

Net effect: single f-m spectrum

f-m spectrum of 0th mode

squelched   f-m spectrum of 1st mode

squelched   f-m spectrum of -1st mode

after inter-action
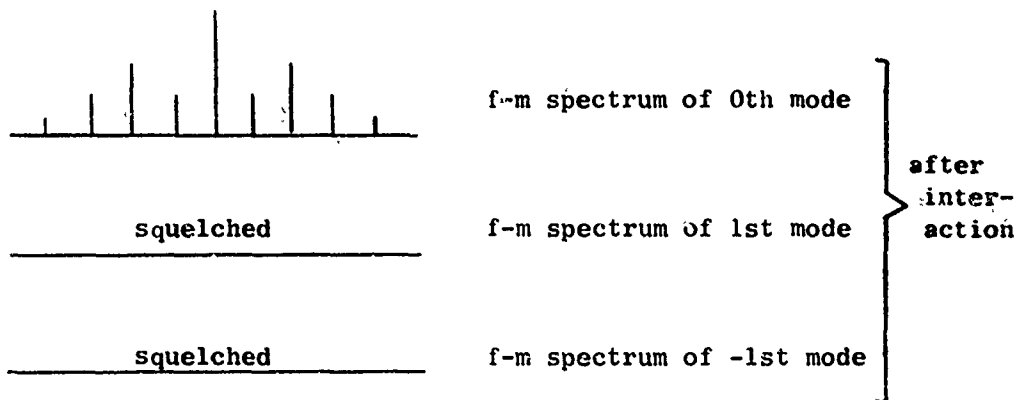
FIG. A-3.   GENERATION OF PURE FREQUENCY MODULATION

z [OOI]

y [OIO]

KDP: $5 \times \frac{1}{2} \times \frac{1}{2}$ cm

BREWSTER ANGLE WINDOWS (QUARTZ)

54°

54°

y'[IIO]

54°

x[IOO]

45°

x'[IIO]
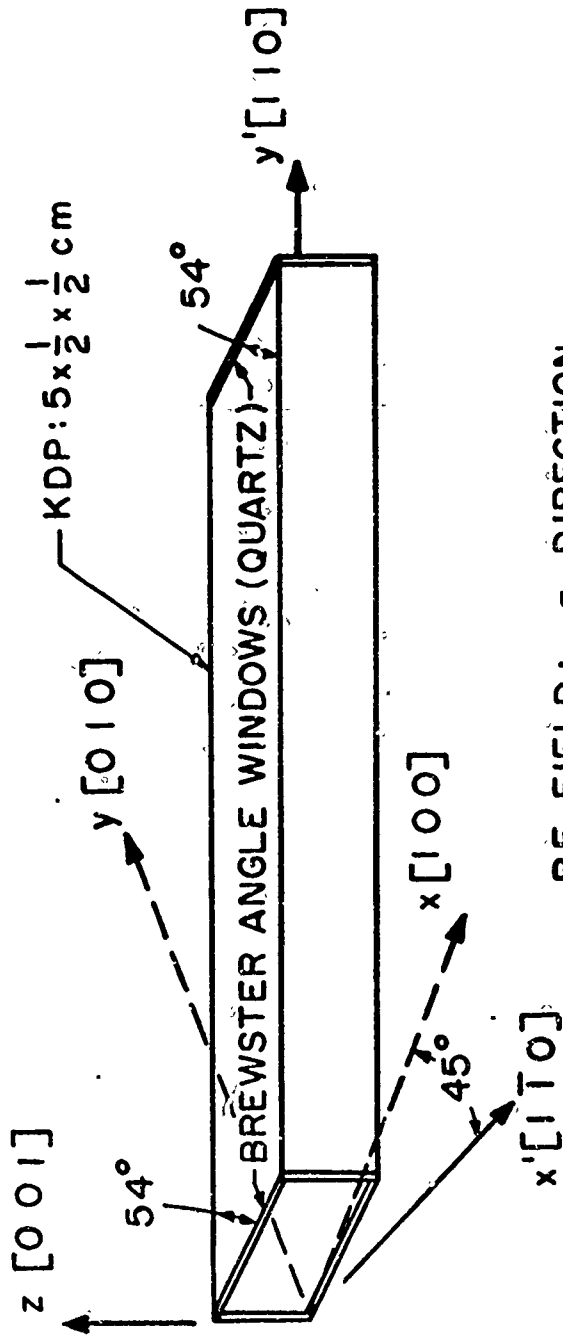
RF FIELD : z DIRECTION

OPTICAL POLARIZATION : x' DIRECTION

OPTICAL PROPAGATION : y' DIRECTION

FIG. A-4. MODULATOR CRYSTAL
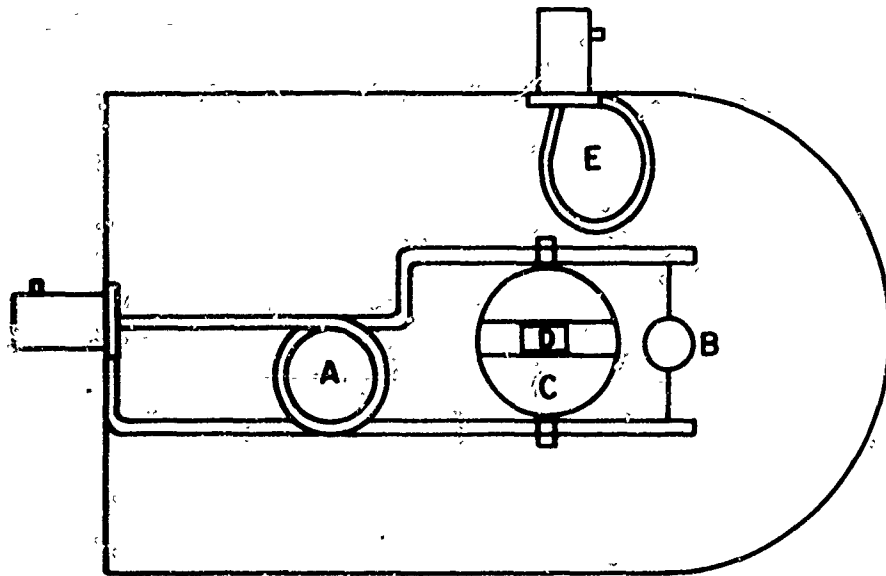
A. RF matching coil

B. RF tuning capacitor

C. Boron nitride for thermal stability

D. Modulator

E. Pickup loop to monitor modulation voltage

FIG. A-5. MODULATOR BOX

the modulator is mounted in a cylinder of boron nitride, which has a high thermal conductivity while being an electrical insulator, so that we may minimize heating effects at high r-f power levels. A loop of wire placed next to the modulator provides a convenient method of monitoring the modulator voltage and thus the optical length as a function of time.

The active medium is a Spectra-Physics Model 116 He-Ne plasma tube, operating at 6328 Å. The tube is 120 cm long, and gives about 10% single-pass gain, sufficient to allow oscillation with several elements in the cavity. The tube has a central cathode and an anode at each end, so that the effect of gas flow in the tube is minimized, even with d-c excitation.

In order that the laser will oscillate in both directions simultaneously, it is necessary to reduce competition between the two oppositely directed waves for the gain of the active medium. As discussed in detail in Ref. A-1, this may be accomplished by splitting the gain profile into two Doppler broadened curves. The splitting may be done either by using a mixture of two isotopes of neon, or by using magnets (Zeeman splitting). We have chosen the latter, rather than going to the large expense of a custom filled plasma tube.

To achieve a certain amount of mechanical stability, we have placed the entire system on a stable table. The table consists of a 3000-lb. granite block supported by alternating layers of bricks and rug pads. The whole table rests on inner tubes which may be inflated to completely isolate the system from earth-borne vibrations. A one-inch aluminum plate which was originally used to facilitate mounting of optical elements was removed when we discovered that it exhibited strong mechanical resonances. Optical elements are now set directly on the granite by means of heavy brass bases.

To minimize effects of wind currents, and to provide dust protection, the system is covered by a box consisting of mylar on a wooden frame. The laser tube is separated from the rest of the system by a plastic cover which keeps out thermal winds created by the hot filament

and plasma.

Since it would be difficult to rotate the heavy table, some other means is needed to simulate rotation over and above the earth's rotation. This is accomplished by inserting in the cavity a non-reciprocal optical-phase shifter. Two such devices which we have used are a Faraday rotator and a Fresnel drag tube.

The Faraday rotator consists of a quartz rod with a coil of wire wound around it so that a d-c magnetic field may be applied along the rod. The ends of the rod are optically contacted to Fresnel rhombs which serve to convert linearly polarized light to circularly polarized light. When a magnetic field is applied, the Faraday effect causes light traveling in one direction through the rod to experience a phase shift which is different from that experienced by light traveling in the opposite direction. This produces an observable frequency beat between the counter-rotating waves, and thus has the same effect as ring rotation.

The Fresnel drag tube is simply a tube with Brewster angle windows on the ends and inlet and outlet hoses, so that gas may flow along the laser beam. The flowing gas has different indices of refraction in the opposite directions, and so simulates rotation.

A third method of rotation simulation has been used in some of our experiments, utilizing the inherent non-reciprocity of phase modulation, as will be discussed later

The geometries of the ring with the Faraday cell and with the Fresnel drag tube are given in Figs. A-6 and A-7 respectively For both cases, Eq. 1 gives a beat frequency of 1 kHz per mrd/sec rotation. The rotation rate of the earth would then correspond to a 50 Hz beat.

The three corner mirrors are multilayer dielectric mirrors, coated for high reflectivity at normal incidence. With our horizontal polarization and relatively large incidence angles, we estimate a loss of 0.1 to 0.5 percent through each mirror This transmitted
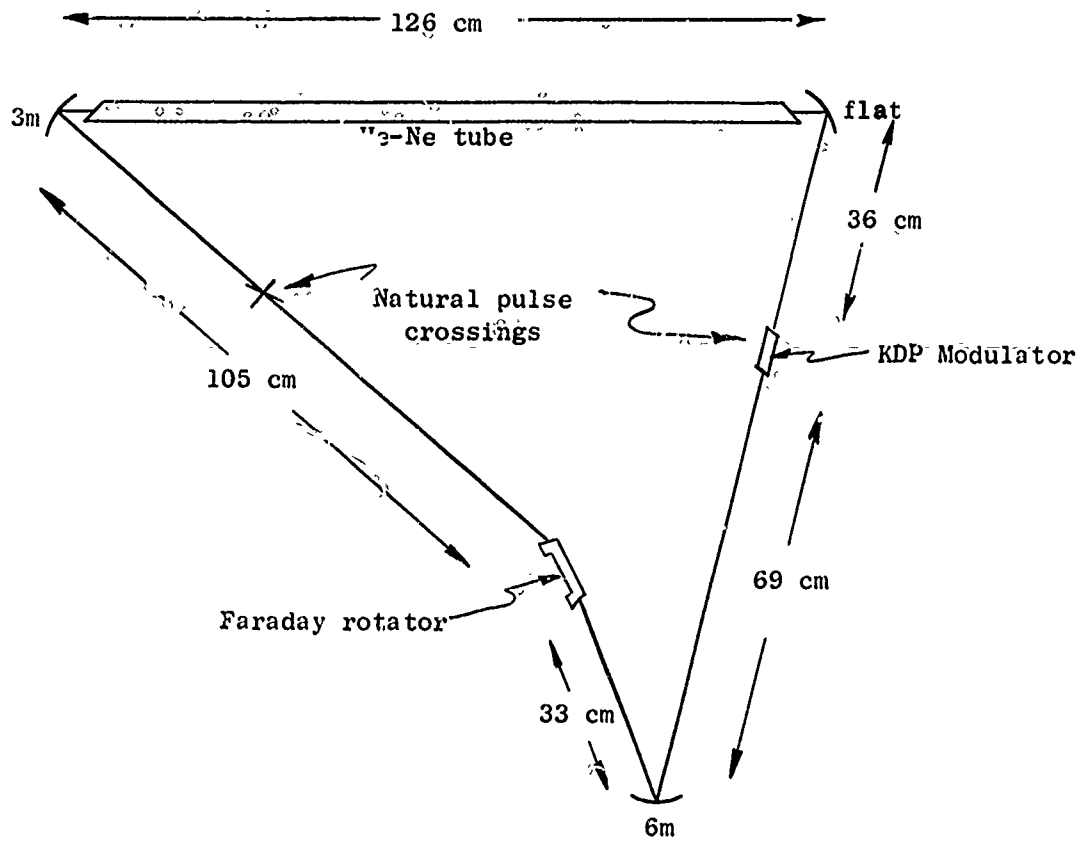
- 1 -

FIG. A-6. RING LASER GEOMETRY WITH PHASE MODULATION
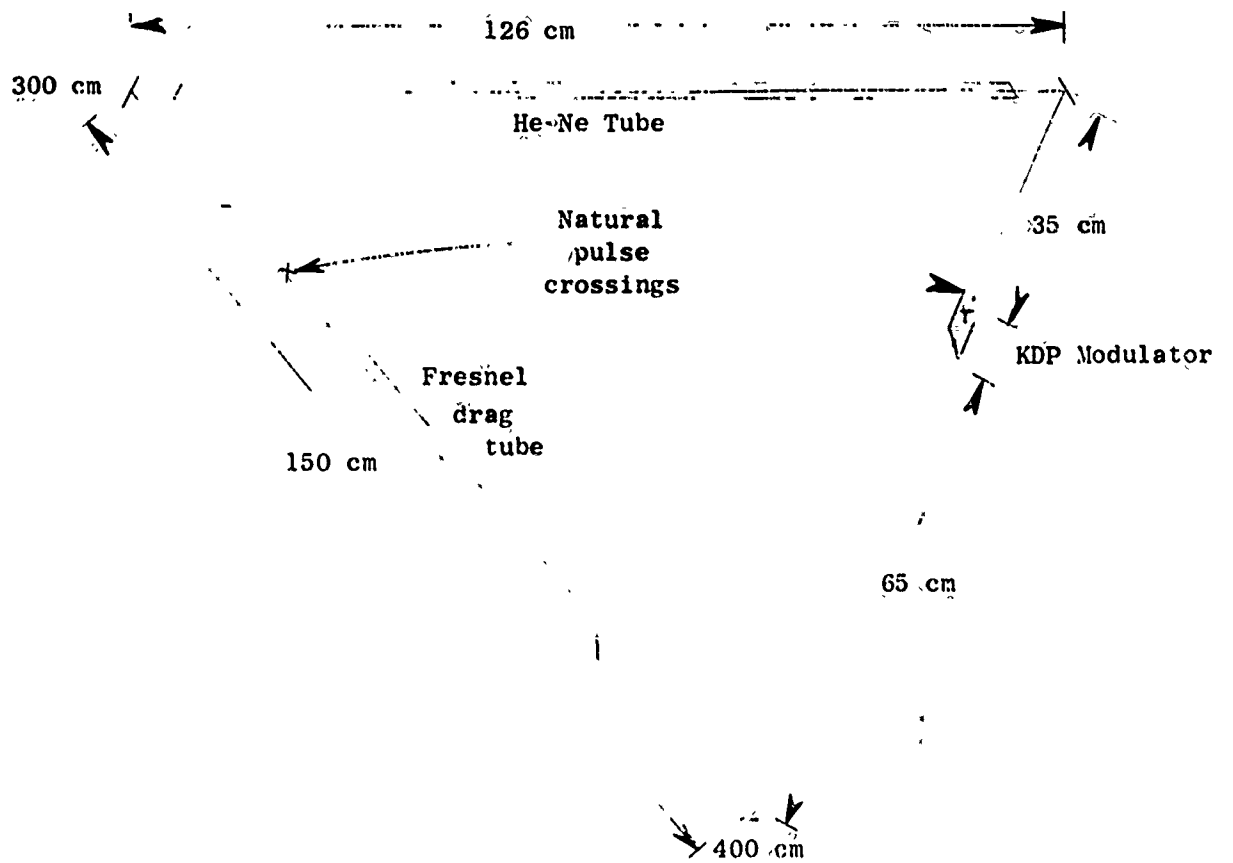AND FARADAY ROTATION

FIG. A-7. RING GEOMETRY WITH PHASE MODULATION
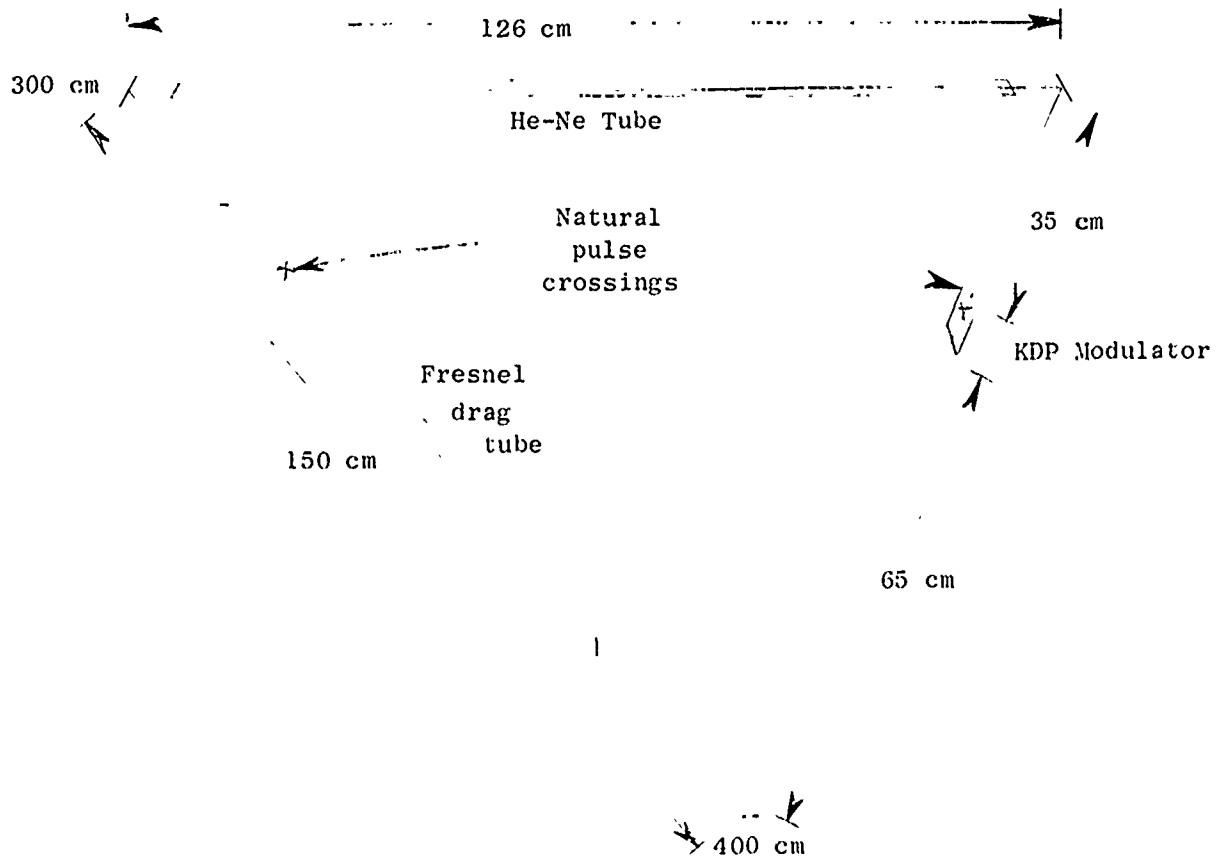AND FRESNEL DRAG

FIG. A-7. RING GEOMETRY WITH PHASE MODULATION
AND FRESNEL DRAG

light, along with light reflected from Brewster windows, is used to
monitor various parameters of the system: output beams from both
directions, with appropriate delay, are combined using a beam-splitter
and low frequency photo-diode to measure the beat frequency between
the oppositely-directed waves. A small amount of light in the combiner
system is fed into photo-diodes to monitor the intensity of the two
waves. Other output beams, one from each direction, are focussed
simultaneously on a PIN photo-diode to monitor the narrow pulses pro-
duced by the modulation. At times a scanning interferometer is used
to look at the optical spectrum, and/or a spectrum analyser is used
to study the r-f beat spectrum.

4.   PULSED OPERATION-RESULTS

    a,   Types of Pulsing

         Experiments were conducted with the modulator placed at the
natural crossing discussed above. By adjusting the modulator fre-
quency and amplitude, we were able to produce nearly all of the types
of pulsing shown in Table A-1. The exception is that with the mod-
ulator at the natural crossing, oppositely-directed pulses tend to
cross in it so that pulses of types 10 and 11 do not occur.

         A map of pulsing type as a function of modulator frequency
and amplitude is given in Fig. A-8. The region identified as produ-
cing single pulses in both directions will also occasionally produce
doubles in one direction, with the other extinguished (types 6, 7).
However, if the modulator is properly placed very close to the natural
crossing, types 6 and 7 will rarely occur, presumably because the
magnets reduce the competition between pulses travelling in opposite
directions, but not between these in the same direction.

         As one would expect, there is very little preference for one
direction over the other, nor for single pulses to arrive at one
modulator phase rather than the other. The resulting direction or
phase depends upon initial conditions, so that stable pulses may be
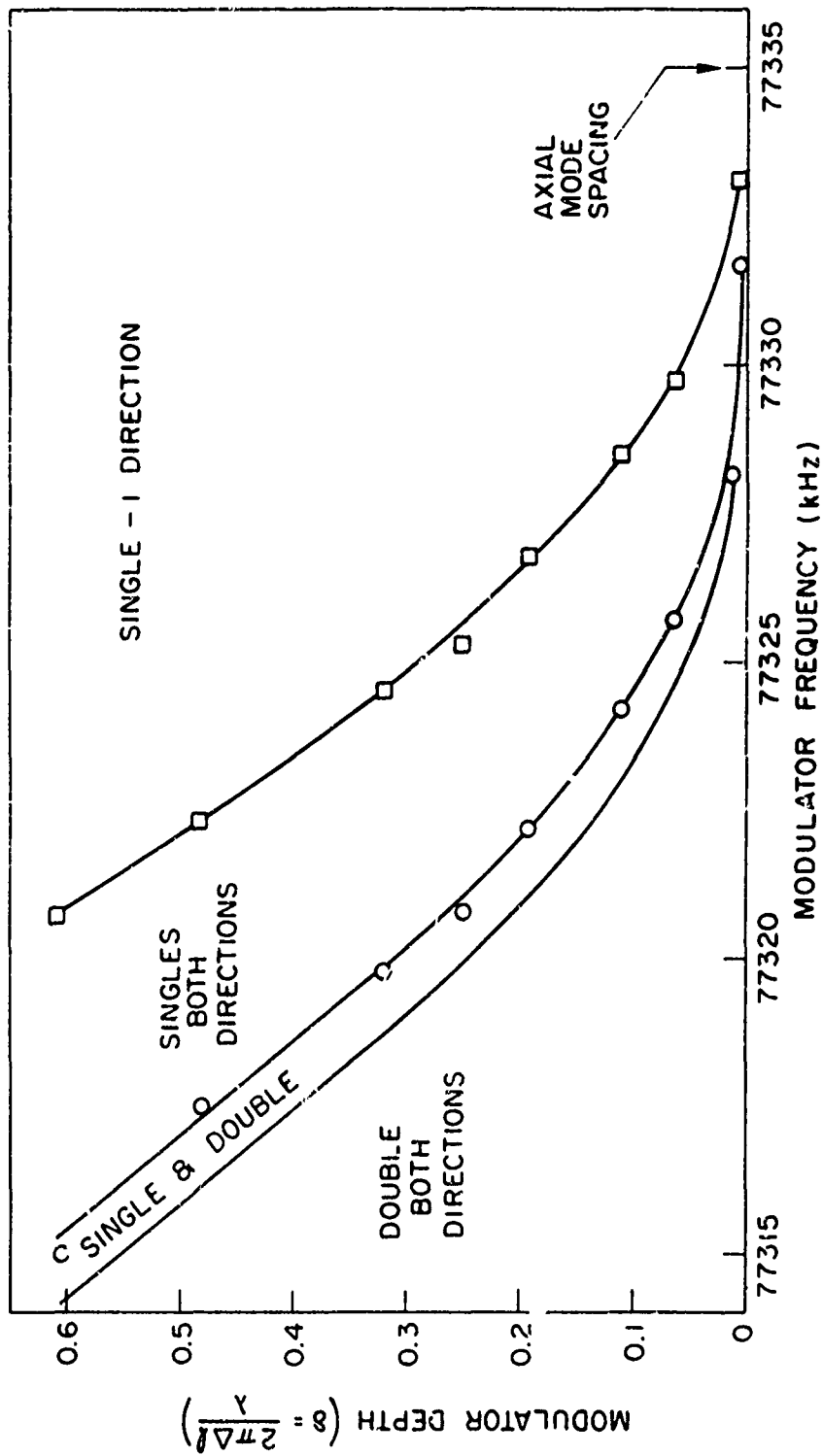produced in either direction or either phase.

FIG. A-8. MAP OF PULSING TYPES

We note in Fig. A-8 that more pulses occur as the modulator
frequency is decreased, and in fact, there is never more than a single
pulse in the ring for frequencie, higher than axial mode spacing.
This effect may be a result of the fact that, in order to keep in step
with the modulator at higher frequencies, a pulse must travel faster.
This can occur if saturation of the active medium favors the front of
the pulse, which can only happen if the saturated medium has time to
relax between pulses, hence fewer pulses at higher frequencies. The
behavior of Fig. A-8 with increasing modulator depth is not understood.

b. Offset

In the case of single pulses in both directions, we have
studied the beat frequency between the oppositely-directed waves.
There exists an offset frequency, or nonzero beat in absence of sim-
ulated rotation. This offset is a function of the position of the
modulator, as is shown in Figs. A-9 and A-10.

We note that for a particular modulator arrival phase, the
offset changes linearly with modulator position, and the slope is
nearly independent of modulator depth (approximately $3\frac{1}{2}$ kHz/cm). We
note further that at any particular modulator position, the offset
for O phase is nearly   al and opposite to that for Π.

These effects can 'e explained by the fact that the mod-
ulator's optical length is a function of time, and for small tunings
of the modulator frequency below axial mode spacing, the pulses arrive
at the modulator slightly before O or Π. Thus if the modulator
position moves slightly away from the natural crossing, the oppositely-
directed pulses will not arrive exactly simultaneously, will see diff-
erent optical lengths, and hence, will have different optical fre-
quencies.

One would expect, then, that the slope of the offset vs
position curves should be a strong function of modulator depth, as
this represents a scale factor for the optical length. A probable
explanation is that, at stronger modulation, the pulse-crossing
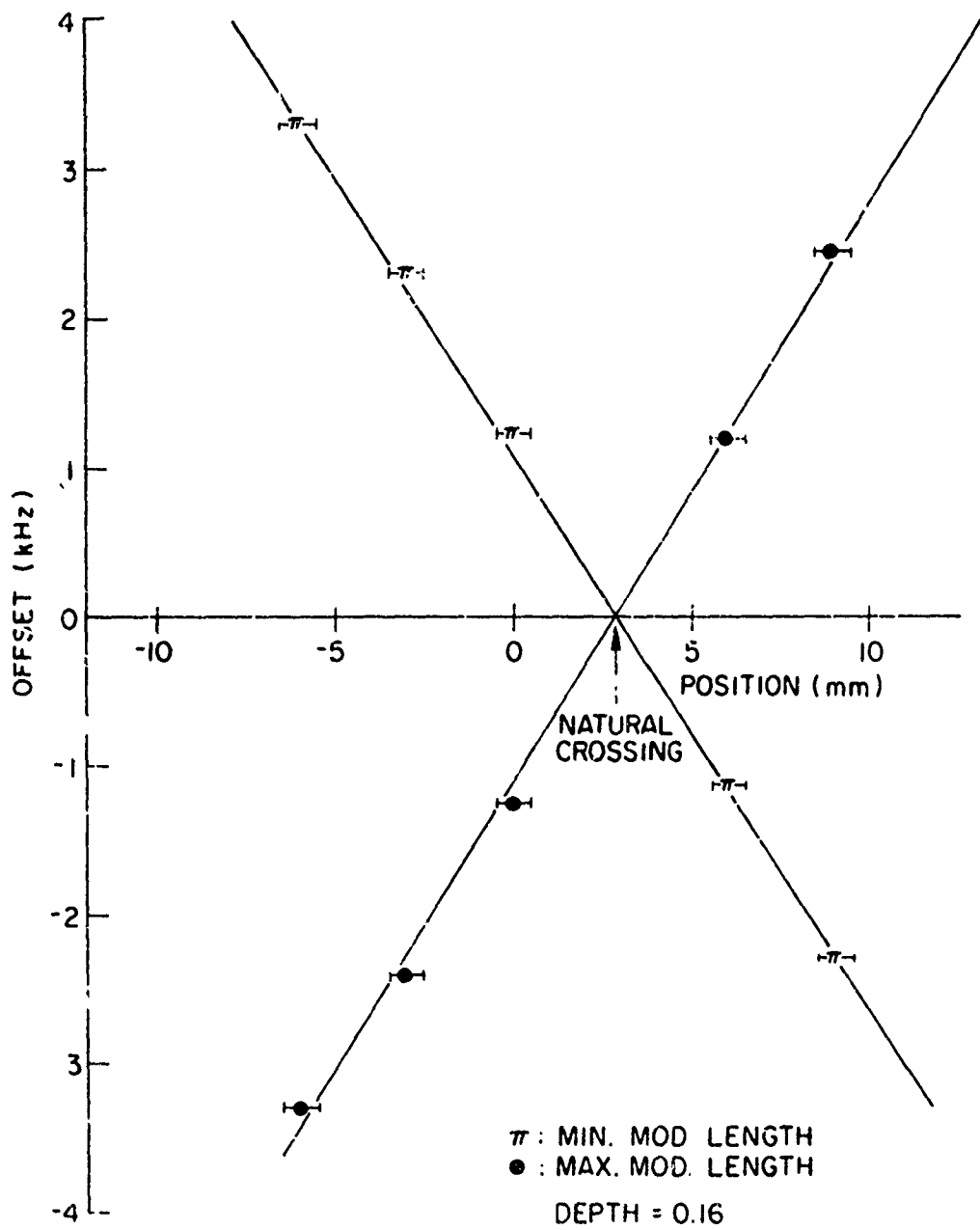position is more closely tied to the modulator, so that the pulses

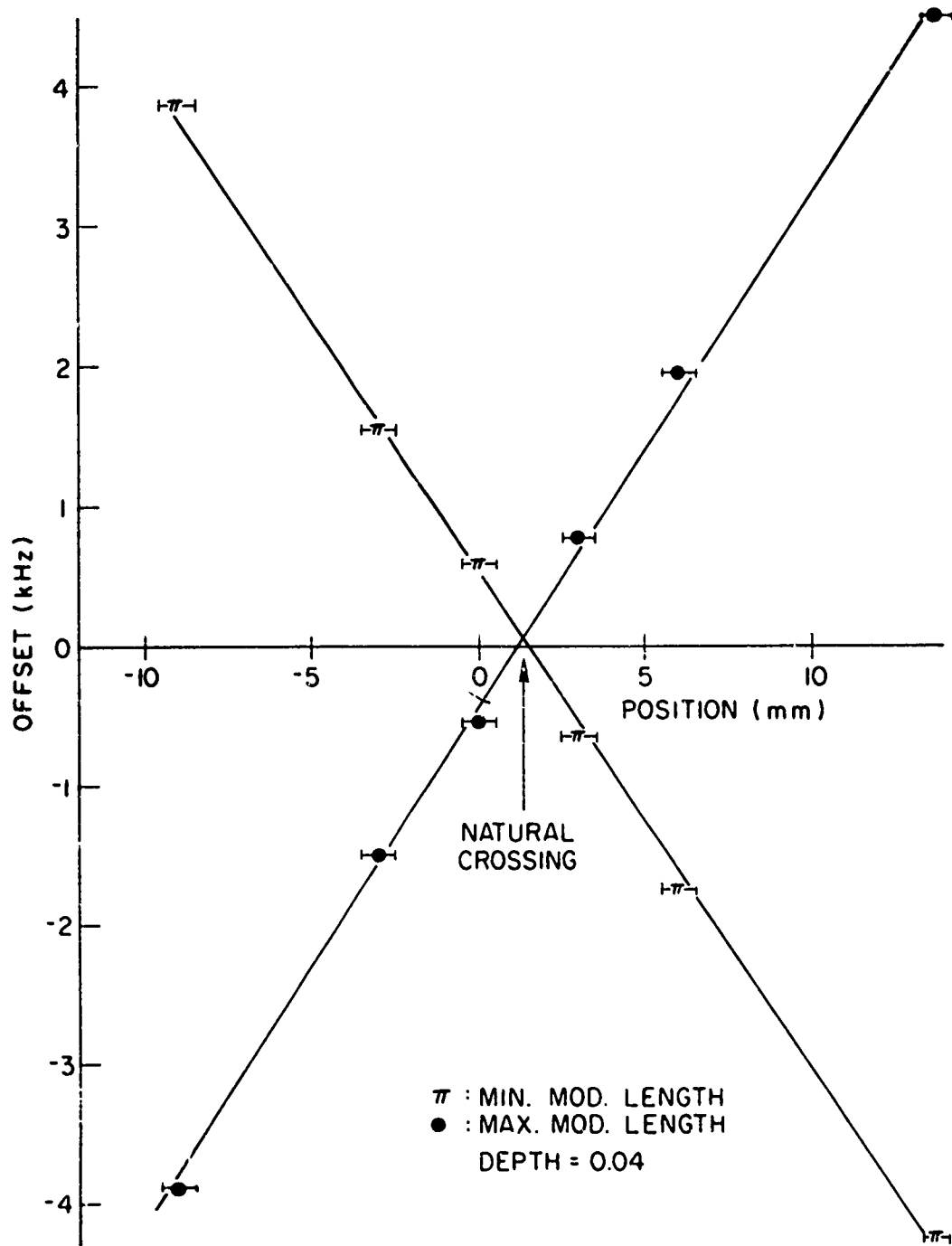FIG. A-9. OFFSET VS. MODULATOR POSITION (Medium Depth)

FIG. A-10. OFFSET VS. MODULATOR POSITION (Low Depth)

do not arrive at the modulator as far apart as at lower depths, an effect which just cancels the length change.

If the offsets for O and Π were exactly equal and opposite, there would be no difficulty, as then one need only measure the beats at both phases, add and divide by two. Unfortunately, this is not the case. Fig. A-11 shows the non-reciprocity of the beat, which in the ideal case would be equal to the beat induced by earth rotation, shown dotted in Fig. A-11. We note that the non-reciprocity is a function of modulator position. Previous data, taken under conditions of higher loss, showed very little variation of non-reciprocity with modulator position over the same range; however, this non-reciprocity could not be accounted for by earth rotation either.

It is clear that the O and Π cases are treated differently by the system. The difference results from the fact stated above that for a small detuning of the modulator frequency below axial mode spacing, as required to produce pulses in both directions, the pulses will arrive at the modulator slightly ahead of the stationary phase points O or Π. Thus the pulses see a slight time variation of optical length and undergo a Doppler shift in frequency. The spectrum is shifted down in frequency for O and up for Π. What this means is that if the gain spectrum of the active medium is not symmetrical, then the spectra of the two pulses will not have identical or mirror shapes. There is reason to believe that such an asymmetry is introduced by any means of reducing competition between oppositely-directed waves, using either magnets or a mixture of isotopes.

The mechanism by which a slight difference in spectral content between the O and Π pulses produces a non-reciprocity in the offset is believed to be as follows: The optical beam diameter, and hence the power density, is nonuniform along the length of the active medium. Therefore, because of nonlinear saturation of the medium, the position of the effective gain center will depend upon the detailed nature of the amplified signal. The result will be that natural crossing position as determined by the medium may be pulled depending upon
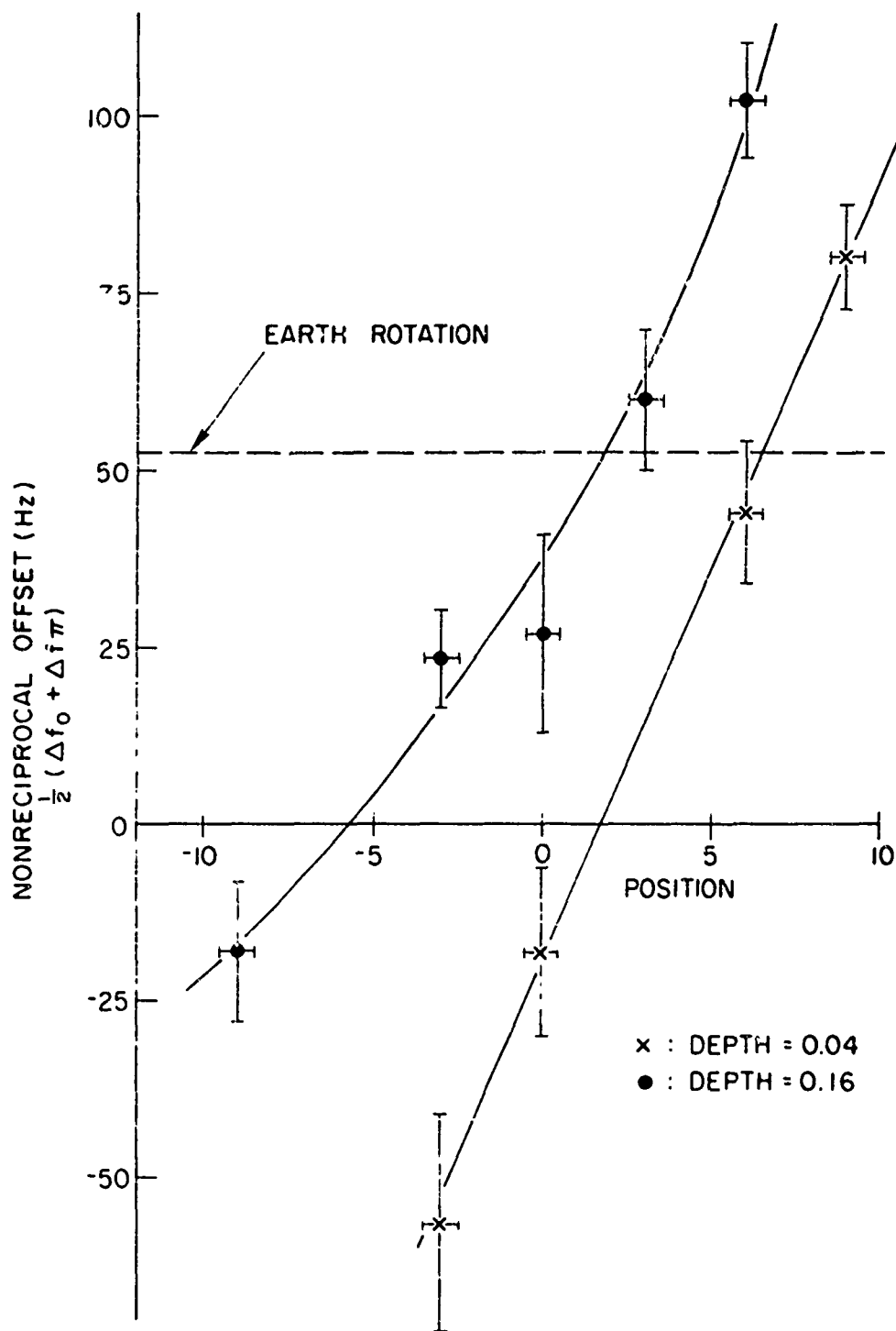
FIG. A-11. NONRECIPROCAL OFFSET VS. POSITION

the detailed shape of the pulses. A shift in the natural crossing of the O pulses relative to that of the II pulses of only approximately 0.1 mm can account for the non-reciprocities seen in Fig. A-11. A comparison of Figs. A-9 and A-10 shows that with nothing changed except the modulator depth, the natural crossing actually moves by millimeters. This result is repeatable, and in fact, the natural crossing is found to move whenever almost any parameter of the system is changed.

c. Rotation Sensing and Locking

The beat frequency between oppositely-directed waves has been measured as a function of simulated rotation rate using the Faraday cell. The result, plotted in Figs. A-12 and A-13, is very surprising. In the O phase case, where the pulses arrive at the modulator near maximum length, the beat is linear with rotation down to about 500 Hz, at which point the two waves become locked together in frequency and the beat signal disappears. This is as one would expect. However, in the II phase case, although the beat signal becomes very noisy and distorted below about 200 Hz, locking never occurs, and the measured beat frequency is linear with rotation over the entire range!

Another, and possibly related, point is that the O phase case, where locking occurs, shows hysteresis effects. Once locking has occurred, it is not possible to produce unlocking unless the simulated rotation is raised to a very high value, corresponding to a beat of about 10 kHz. In addition, when locking has occurred at O, if the beam is interrupted and switched to II, locking will remain for several seconds, after which the beat frequency will gradually increase to the proper value. Finally, if locking has occurred at O phase and the laser beam or modulator beam is interrupted, the locking will remain, even with applied rotation, provided the O phase condition is reestablished within several seconds.

The hysteresis effect can be explained in terms of striations which form in the KDP in the presence of an optical standing wave. The striations produce enhanced reflection which increases the coupling
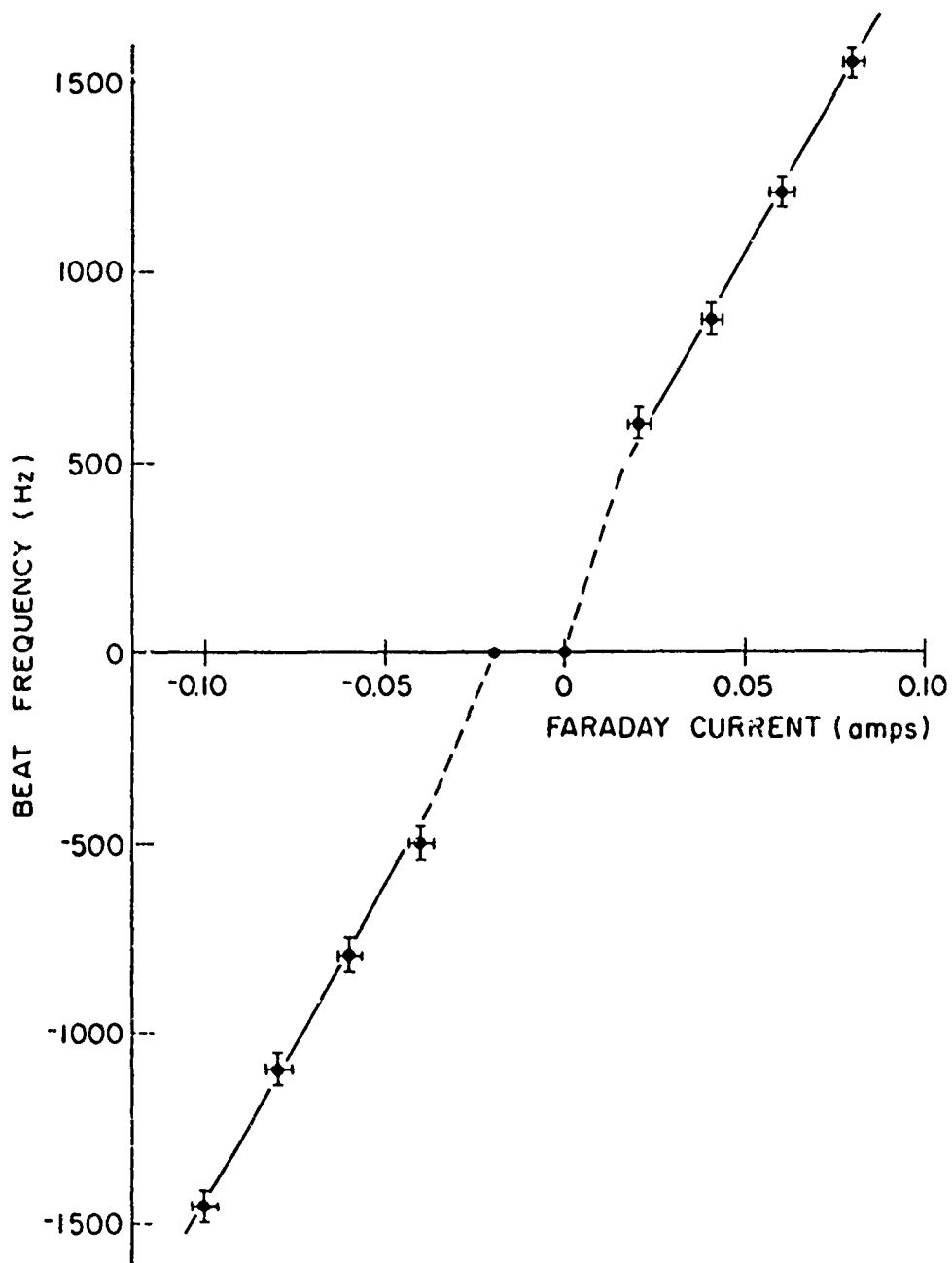
FIG. A-12. BEAT FREQUENCY VS FARADAY
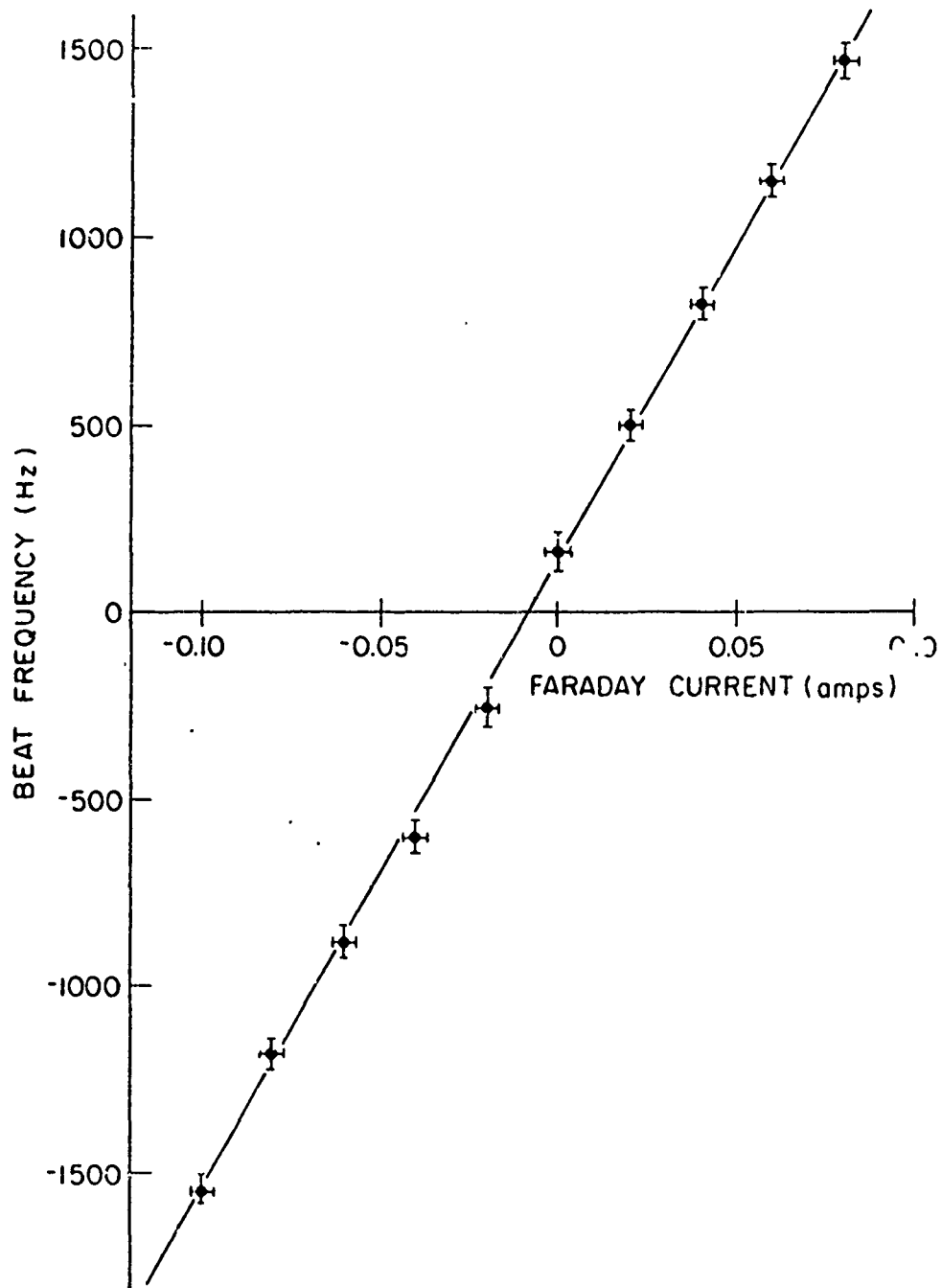CURRENT (0-Phase Case)

FIG. A-13.   BEAT FREQUENCY VS FARADAY
CURRENT (II-Phase Case)

between the oppositely-directed waves, and thus maintaining the locking.

The striation effect, as well as an experiment to study the phenomenon and a discussion of the mechanism, has been written up as a letter [Ref. A-4].

The striation effect offers a possible explanation of the absence of locking in the Π phase case. Perhaps, under the conditions which would produce locking, striations build up which are of such a phase that their reflection cancels all other reflections, producing unlocking. This would then correspond to a highly distorted beat signal such as we have observed. However, we have been unable to develop a rigorous theory which confirms this hypothesis.

In any event, the absence of locking shows promise as a measure of rotation rates, except for two present drawbacks: first, there is the inherent offset discussed above which prevents absolute rate measurement; and second, the noise and distortion limit accuracy to rates of about 0.05 mrd/sec. This compares extremely favorably with the same cavity without modulation, where no beat is visible below several mrd/sec.

5. FREQUENCY MODULATION

Some effort has been given to operation of the ring laser in the f-m region, with little success. We have achieved mode locking into a single f-m spectrum which appears to be quite stable. However, attempts to measure beat frequencies have been unsuccessful. Work is continuing in this area. There is some question as to what is the proper modulator position for best f-m operation, as well as the effect of cavity length variations. News of any progress in this area will be available to the Air Force.

6. CONCLUSIONS

The ring laser with phase modulation shows promise as a detector of low rotation rates. We have found a condition in which locking does not occur between oppositely-directed waves. The utility is

somewhat reduced by an inherent offset which prevents absolute rotation measurer ents, and the sensitivity is limited by noise and distortion. However, we have seen an increase in sensitivity by a factor of 20 or more compared with the same device without modulation.

This project has proved valuable in providing enhanced understanding of phase modulation and ring lasers in general as well as mechanisms within the modulating crystal itself.

Suggestions for further study include continued effort in the f-m region (which we are undertaking in this laboratory), use of other modulating crystals, and combination of techniques developed here with those commonly used in a single frequency ring.

APPENDIX A REFERENCES

A-1. N. Buholz, "Synchronous Amplitude Modulation of a Multimode Ring Laser," Ph.D. Dissertation, Department of Electrical Engineering, Stanford University, Stanford, California, supported by Air Force Contract No. F33615-67-C-1245, 1968.

A-2. S.E. Harris and O.P. McDuff, *IEEE J. Quantum Electronics*, vol. QE-1, p. 245, 1965.

A-3. E.O. Amman, B.J. McMurty, and M.K. Oshman, *IEEE J. Quantum Electronics*, vol. QE-1, p. 263, 1965.

A-4. S.I. Wax, M. Chodorow, and H.E. Puthoff, "Optical Damage in KDP," *Applied Phys Letters*, vol. 16, p. 157, 1970.

IV. SURFACE WAVE PARAMETRIC AMPLIFICATION

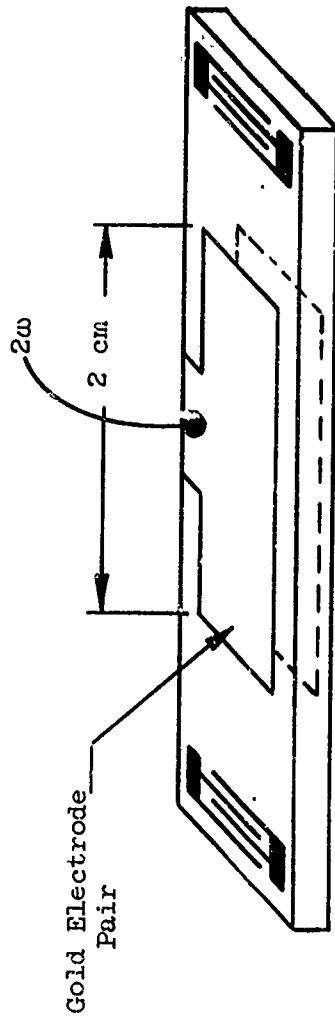(G. S. Kino and M. V. Luukkala)

A. INTRODUCTION

This project is concerned with the study of parametric interactions
between surface acoustic waves. The use of parametric interactions
themselves can lead to new kinds of parametric amplifiers, and new
types of parametric oscillators. The oscillators have the advantage
that a surface acoustic wave can be induced into the medium without
the use of a fine pitched transducer

Surface acoustic waves are particularly suitable for the study
of nonlinear effects. Because the surface waves are confined to a
thin layer of the crystal, the energy density associated with the
wave tends to be very high. For a 200 MHz surface wave this layer
thickness is approximately $5\ \mu m$. Thus, if we compare the power density
in a width of 1 mm, with that in a volume wave of area 1 mm^2, the
power density associated with the surface wave is 400 times larger
Thus if strong nonlinearities occur with a volume wave at an input
power level of a few hundred watts, the power level to obtain the same
degree of nonlinearity in a surface wave will be of the order of one
or two watts. At such power levels the acoustic strain is in the
range 10^{-4} -10^{-3}. Two kinds of nonlinearities are involved 1) an
acoustic nonlinearity which arises because when the strain is large the
medium no longer obeys Hook s law, 2) an effect in piezoelectric crystals
where the piezoelectric stiffening of the ultrasonic wave is fairly
large, in which the dielectric and piezoelectric constants may change
with the field and with them also the stiffening and the sound velocity
It is felt, although we do not have definite proof that the first
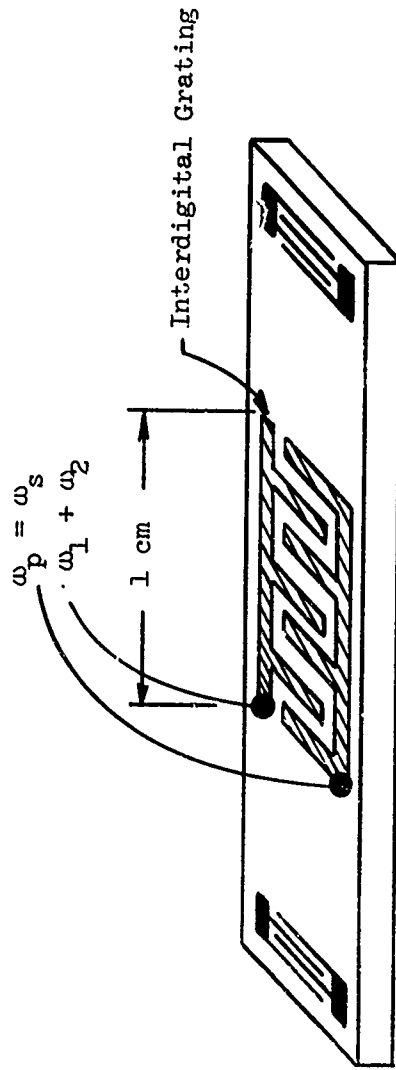type of nonlinearity is the one of most importance

B. PARAMETRIC INTERACTION THEORY

We initially considered the interaction between three signals of frequencies ω_1 , ω_2 , ω_3 and propagation constants k_1 , k_2 , k_3 respectively, all propagating in the same direction. Strong inter- actions should be expected in this case when $\omega_3 = \omega_1 + \omega_2$ and $k_3 \approx k_1 + k_2$. In practice, by putting a signal in a surface wave transducer at a frequency ω_1 , we were able to observe second harmonic generation, and were able to observe higher harmonics as well. It was intended originally to make a traveling wave parametric amplifier by putting a pump in at the frequency ω_3 and observing growing signals and idlers at f equencies ω_1 and ω_2 , respectively. However, because of the presence of higher idlers at frequency $m\omega_1 + n\omega_2$, which interact strongly in this nondispersive medium, parametric amplification was not obtained.

Instead, we have concentrated our efforts in observing and making use of the parametric interactions between two waves propagating in opposite directions which have frequencies ω_1 and ω_2 , and propagation constants k_1 , $-k_2$, respectively. The nonlinear coupling between two acoustic waves of this kind, then, gives rise to an acoustic strain in the medium at a frequency $\omega_3 = \omega_1 + \omega_2$ with a prop gation constant $k_3 = k_1 - k_2$. It will be observed that, because the velocities of the two surface acoustic waves are identical, if $\omega_1 = \omega_2 = \omega$, the output frequency will be 2ω , and the effective propagation constant of the nonlinear component will be zero. Thus, it should be possible to detect the acoustic strain at a frequency 2ω and associated electric field set up in a piezoelectric plate by means of metal films deposited on each side of the slab, as shown in Fig. 1, when signals are introduced into the medium on transducers at each end. Likewise, we would expect that if a signal were placed on the acoustic medium at a frequency ω and a pump input between the metal films at the frequency 2ω , there would be an idler signal generated in the opposite direction at a frequency ω . Then using pulsed signals, it is possible to sort out the idler output separately from the input signal.

2ω

2 cm

Gold Electrode
Pair

YZ-Cut LiNbO$_3$ Delay Rod

(a)

Interdigital Grating

$\omega_p = \omega_s$

$\omega_1 + \omega_2$

1 cm

YZ-Cut LiNbO$_3$ Delay Rod

(b)

FIG 1--Electrode configurations used in the surface wave parametric experiments.

We now consider using coupled mode theory, the situation when a signal of input frequency ω and strength A_s, where the power in the wave is $P_s = 1/2 \, A_s A_s^*$, is induced on an interdigital line and interacts with a uniform field pump at a frequency 2ω. The peak amplitude of the pump field between the two metal films is taken to be E_p. If the idler power is $P_i = 1/2 \, A_i A_i^*$ we find the following coupled mode equations between idler and signal:

$$\frac{dA_s}{dz} + jkA_s + \alpha A_s = \frac{jk\lambda E_r}{4} A_i^* \qquad (1)$$

$$\frac{dA_i^*}{dz} + jkA_i^* - \alpha A_i = \frac{jk\lambda^* E_r^*}{4} A_s \qquad (2)$$

where k is the real part of the propagation constant of signal and idler waves, and α is their attenuation per unit length. The parameter λ is a coupling constant, which can be measured directly by application of a dc field to the plate. In this case, with dc field applied, it is easy to show from expressions like Eq. (1) that the coupling equation is

$$\frac{dA_s}{dz} + jkA_s = jk\lambda E_0 A_s \qquad (3)$$

This yields the result that the perturbation in acoustic velocity due to the application of a dc field E_0 is

$$\frac{\Delta v}{v} = \lambda E_0 \qquad (4)$$

When $\alpha < k\lambda E_p | 2$ it can be shown that

$$|A_s(z)| = |A_s(0)| \frac{\cos[\Gamma(\ell - z) - \phi]}{\cos(\Gamma\ell - \phi)} \qquad (5)$$

- 50 -

and

$$|A_i(z)| \quad - \quad |A_s(0)| \; \frac{\sin \Gamma(\ell-z)}{\cos \, (\Gamma \ell - \phi)} \qquad (6)$$

where

$$\Gamma \;=\; k^2(\lambda E_p/4)^2 - \alpha^2 \qquad (7)$$

and

$$\tan \dot{\phi} \;=\; \alpha/\Gamma \qquad (8)$$

and ℓ is the interaction length. It will be seen that if α is small, oscillations take place if the length of the system is large enough, or the power in the pump large enough so that $\Gamma \ell > \pi/2$. On the other hand, if the attenuation is large, it can be shown that when $\alpha \gg \Gamma$ the ratio of the idler signal at $z = 0$ to the input signal is given by the relationship

$$\frac{A_i(0)}{A_s(0)} \;=\; \frac{k\lambda E_p}{8\alpha} \;. \qquad (9)$$

Thus, the value of λ can be measured relatively simply by rf measurements or by dc measurements.

More generally, if the signal and idler frequencies are not equal, the pump must have an equivalent propagation constant

$$k_p \;=\; k_3 \;=\; k_1 - k_2 \;=\; \frac{\omega_1 - \omega_2}{v_a} \qquad (10)$$

where v_a is the velocity of the acoustic wave. As

$$\omega_p \;=\; \omega_3 \;=\; \omega_1 + \omega_2 \qquad (11)$$

it follows that

$$\omega_2 = \frac{\omega_p}{2} \left[1 - (v_a k_p / \omega_p) \right] , \qquad (12)$$

and

$$\omega_1 = \frac{\omega_p}{2} \left[1 + (v_a k_p / \omega_p) \right] \qquad (13)$$

Thus in this case the pump could be introduced on a relatively coarse
transducer with a pitch corresponding to the difference in propagation
constants between the two waves. However, now, by inducing the pump
on a transducer it is possible to obtain much larger fields between
the interdigital fingers which may be only 10-20 μ apart rather than
between the two metal faces which are of the order of 1/2 mm apart. It
would be expected that the use of a coarse transducer for the pump
would give much better sensitivity and it would be easier to make a
parametric oscillator this way

C. EXPERIMENTAL RESULTS ON PARAMETRIC SURFACE WAVE INTERACTIONS

The experiments were carried out using the configurations shown
in Fig. 1a and b (The same configurations were also used in another
experiment to be described later). In Fig. 1b the interdigital
periodicity is determined by the k_p-vector. The pump was connected
to the central plate electrode through a coaxial resonator or stub
tuner. In the case of Fig. 1a, two ten finger-pair, 105 MHz transducers
were used at the end of the rods, and the length of the continuous
central electrode was 6 cm

Using the configuration of Fig. 1a, a signal pulse at 105 MHz
was inserted on the input transducer. A pulse of rf at 210 MHz was
inserted on the center plate; the average pump power was a few watts.
A return idler signal at 105 MHz was observed but because (1) it was
partially masked by the much larger ingoing signal pulse, and (2) plate
mode oscillations at the subharmonic frequency were excited by the pump,
no good measurements of the amplitude of the surface wave idler could

be carried out. When the signal and pump pulses were shortened in
order to separate the idler and signal pulses conveniently on the
receiver, the signal-to-noise ratio worsened as predicted by Eq. (2).
The fact that subharmonic oscillations occurred even without an input
signal present showed that the postulated nonlinearities were relatively
strong. By covering the surface of the delay line with various absorbing
materials, and using electrostatic probes it was shown that the
subharmonic oscillations that were excited were volume wave plate modes,
with the surface wave transducers acting as poor couplers to these
volume waves. The oscillating behavior repeated itself at about 2.5 MHz
intervals, which roughly corresponded to the thickness of the crystal
From this it was concluded that subharmonic plate waves were excited
through the acoustic nonlinearity It was also observed, that the
subharmonic oscillations died away within 1 or 2 μsec when the pump was
turned off. This indicates a rather lossy wave with a high nonlinear
coupling, which may be the case with a plate wave near the cutoff.
Because the subharmonic oscillations were not very susceptible to
systematic investigation and because of the large number of possible
plate modes present, it was decided to redesign the system to emphasize
surface wave interactions

The experiment was repeated using the configuration in Fig 1
with a 30 finger-pair 105 MHz interdigital transducer as the pumping
electrode In this way the pumping field would be concentrated at
the surface and a better filling factor would result The 105 MHz
transducer corresponded to a k_p-vector of 1.9×10^5 cm^{-1} corresponding
to signal and idler frequencies at 85 and 185 MHz respectively with
a pump frequency of 270 MHz The signal and idler were detected using
a 220 MHz, 4 finger-pair transducer at the end of the rod

A strong idler was detected and the coupling coefficient was
measured from the idler amplitude using an expression similar to Eq (2)
The measured value about $\sim 1 \times 10^{-10}$ is somewhat unreliable,
mainly because the measurement of the relevant parameters could not
be carried out accurately as both the signal and idler frequencies were
well outside the passband of the input transducers However the measured

value of λ is in the same range as the value obtained for volume waves by B. Thompson.

From Eq. (1) it is noted that lossless transmission occurs when $E_p = 4\alpha/\lambda k_s$. If $\alpha \sim 0.8$ dB/cm at 220 MHz, we see that the peak field has to be ~ 120 kV/cm, which tends to be unrealistically high for a grating. It is interesting to note, however, that by using higher frequencies the threshold could be greatly reduced. In the present measurements $E_p \approx 7.5$ kV/cm at 470 MHz.

V. SEMICONDUCTOR FILMS

(G. S.Kino and L. A. Coldren)

A. INTRODUCTION

Last fall a program was initiated in this laboratory to produce thin films of indium antimonide. The primary purpose of this investigation was to provide additional material which could be used in an acoustic surface wave amplifier. InSb was chosen to be flash evaporated in vacuum in view of the relative simplicity of the technique and the large measure of success achieved with this material by other experimenters. Over the past several months apparatus and procedures for producing InSb thin films have been refined. Initially the effort was aimed at making high mobility films ≥ 1 μm in thickness. During the past three months, however, thinner films with parameters suitable for use in a surface wave acoustic amplifier have been sought. Most recently, the work has been directed toward the fabrication of a monolithic acoustic amplifier.

B. EXPERIMENTAL

The most significant result of the early work was that the flash evaporation technique proved successful. This procedure first suggested by Harris and Siegel[1] has proved to be a very successful technique for achieving high quality InSb thin films.[2,3,4] The procedure used here is similar to that used in other laboratories. Granulated InSb source

---

[1] L. Harris and M. Siegel. J. Appl. Phys. 19, 739 (1948).

[2] S. K. Sharma and V. K. Jain, Solid-State Electronics (Pergamon Press, 1968) Vol. 11, pp. 423-428

[3] H. H. Wieder, Solid-State Electronics (Pergamon Press, 1966) Vol. 9, 373-382.

[4] M. H. Francombe and J. E. Johnson, Phys. s of Thin Films (Academic Press, 1969) eds. G. Hass and R.E Thun, Vol. 5, p 176.

material is continuously dropped into a tantalum evaporator which is resistivity preheated to ~ $1600°C$ in vacuum. The sample substrate is maintained at $300-400°C$ to promote oriented crystal growth from the impinging stoichrometrically proportioned vapor.

Using glass substrates supported behind a mask cut in the shape of a Hall sample films ~ 1 μm in thickness were deposited. See Fig. 1 for a schematic of our process. After the sample cooled to $250°C$ air was let [in] to oxidize [and] form [a protective] oxide layer. This was [done to] [prevent the] "peeling-up" of the film during [the etching] [process] [which required] 30-240 [minutes]. The films [obtained] [in these] experiments had max. mobilities ~ 20,000 cm²/V·sec.

Once [we were] [satisfied] that our apparatus and procedure could provide results comparable to those which existed in the literature, it was decided to redirect our goals toward developing films which might be suitable for use in an acoustoelectric surface wave amplifier.

It may be shown that for reasonable acoustic gain, the conductivity-thickness product (σd) for the semiconductor film must be $\lesssim 10$ μ℧ and the drift mobility (μ_D) should be $\gtrsim 300$ cm²/Vsec.[6] It should be pointed out at this stage that these parameters put strict limitations on an InSb film thickness Expressing the conductivity-thickness product as

$$\sigma d = qn\,\mu_D d \quad ,$$

we can solve for the required thickness. Now for $(\sigma d) = 10^5$ μ℧ $q = 1.6 \times 10^{-19}$ C , $n = 3 \times 10^{16}/cm^3$, and $\mu_D = 300$ cm²/Vsec , a maximum usable film thickness is estimated to be $d \lesssim 700$ Å . Figure 2 is a plot of d versus μ_D from the above equation. Lines of constant (σd) are plotted for selected values of n . The experimental dotted curve gives the maximum Hall mobility, μ_H , obtained for a substrate temperature of $400°C$ and no recrystallization. For lower substrate

[5]J. A. Carroll and J. E. Spivak, Solid-State Electronics (Pergamon Press, 1966), Vol. 9, pp. 383-387.
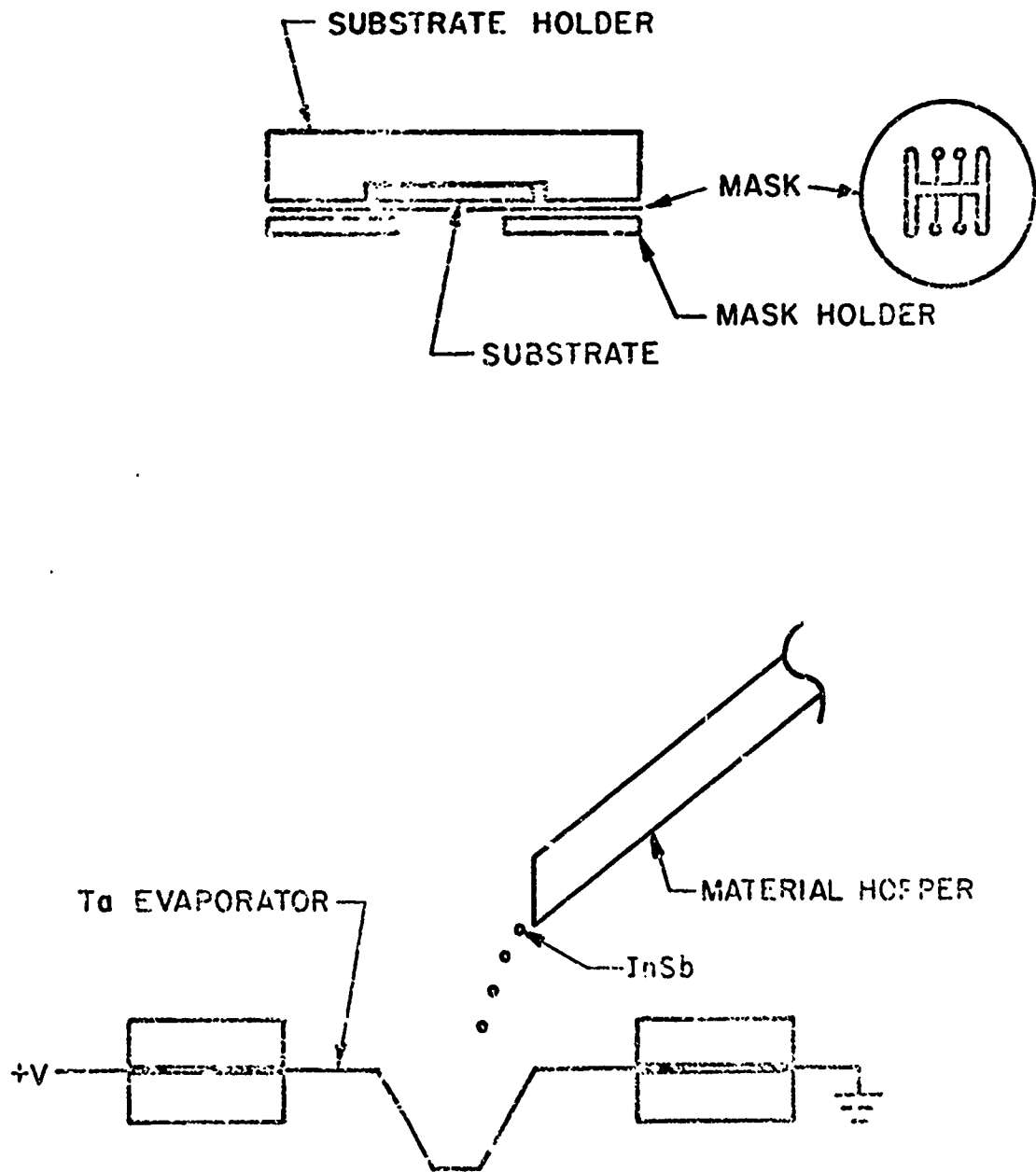
[6]T. M. Reeder, private communication.

FIG. 1-Flash Evaporation Apparatus.

THICKNESS vs MOBILITY FROM $d = \frac{(\sigma d)}{qn}\frac{1}{\mu}$

$\sigma d = (\ )\,\mu\mho$ FOR $n = (\ )\,cm^3$

(2.5) (5) (10) $\longrightarrow$ (2×10^{16})
(5) (10) (20) $\longrightarrow$ (4×10^{16})
(10) (20) (40) $\longrightarrow$ (6×10^{16})

UNRECRYSTALLIZED
MOBILITY LIMIT
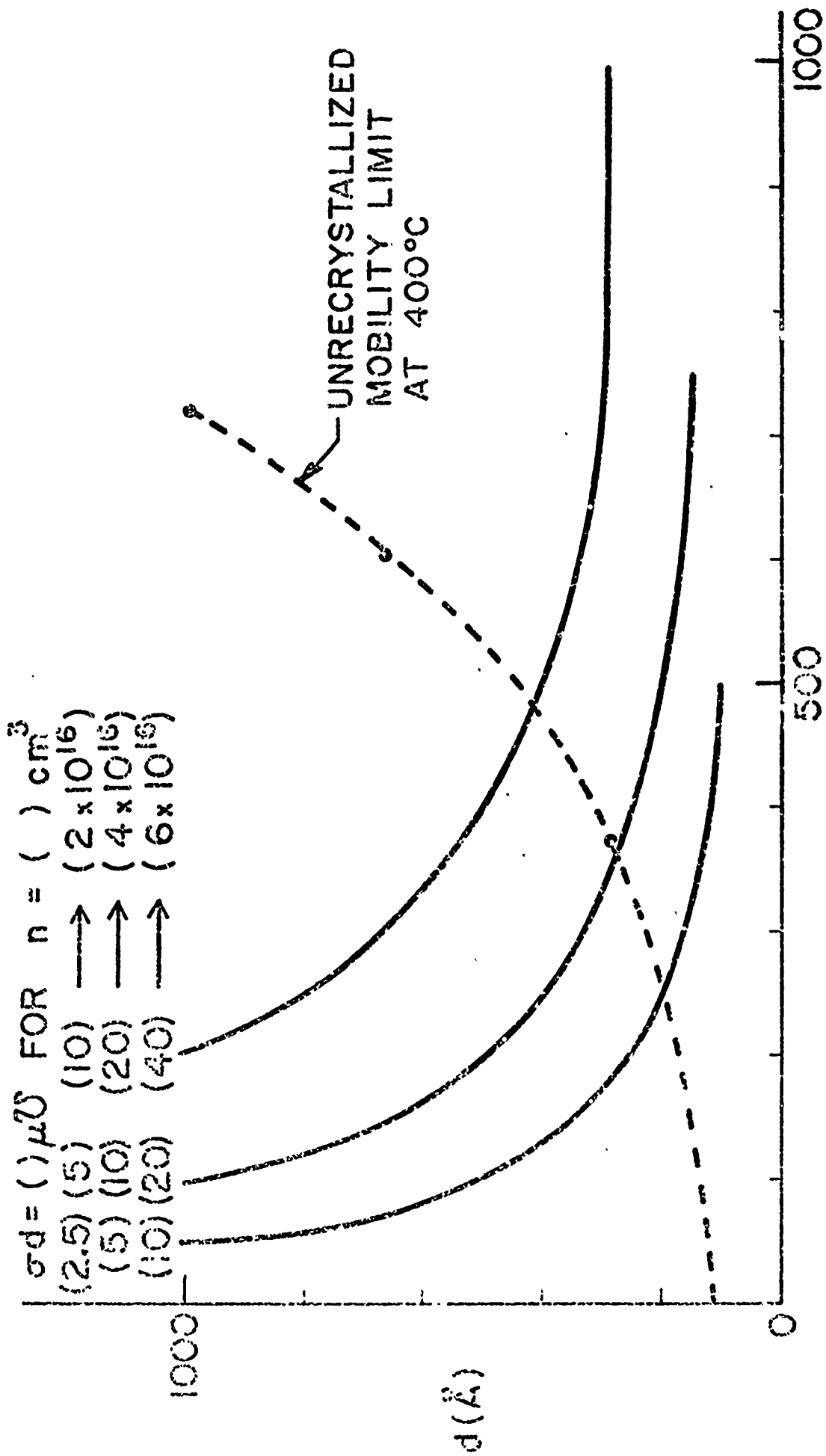AT 400°C

μ

d($\mathring{A}$)

1000

500

1000

FIGURE 2

temperature, lower mobilities are observed due to an increase in the polycrystalline nature of the films. Due to their extreme thinness and a desire for very flat film surfaces the films are no longer re-crystallized following deposition.

To date several films have been deposited on quartz and microscope slide substrates, satisfying the minimum criteria on μ and (σd) . In most cases the procedure yields high purity material. In fact, the carrier concentrations, as estimated from Hall and conductivity measure-ments, are usually within a factor of three from the starting material $(n = 2 \times 10^{16} \ cm^{-3}$ at room temperature). However, in practice diffi-culties arise from variations in thickness despite the installation of a laser transmission monitor. This is primarily because the (σd) pro-duct is quite sensitive to small deviations in thickness It has been observed that the conductivity is also a function of d and, moreover, the first ~ 100 Å of the film is semi-insulating.

The presence of the semi-insulating layer possibly may be explained by the existence of trapping centers associated with substrate-film interface defects. The presence of surface related trapping states also might explain the low carrier concentrations observed at $77^{\circ}K$ with our thinnest samples. Figure 3 gives a plot of conductance versus reciprocal temperature for several samples.

The separated medium surface-wave-acoustic amplifier requires that a semiconductor film be brought to within several hundred angstroms of a piezoelectric material which is propagating an ultrasonic surface wave But, mechanical contact with the piezoelectric delay line must be avoided in the active region. Hence, electrical contacts at the ends of the semiconductor film cannot extend more than a few hundred angstroms from the active surface of the film. To avoid this contacting problem we have been using substrates with beveled ends so that the contact can be made away from the flat surface, as illustrated in Fig 4 Th i over which the film is deposited does not appear to affect the semi-conductor properties.

Another criteria which the film must meet to be suitable for use in this amplifier is an ability to withstand high drift fields. To
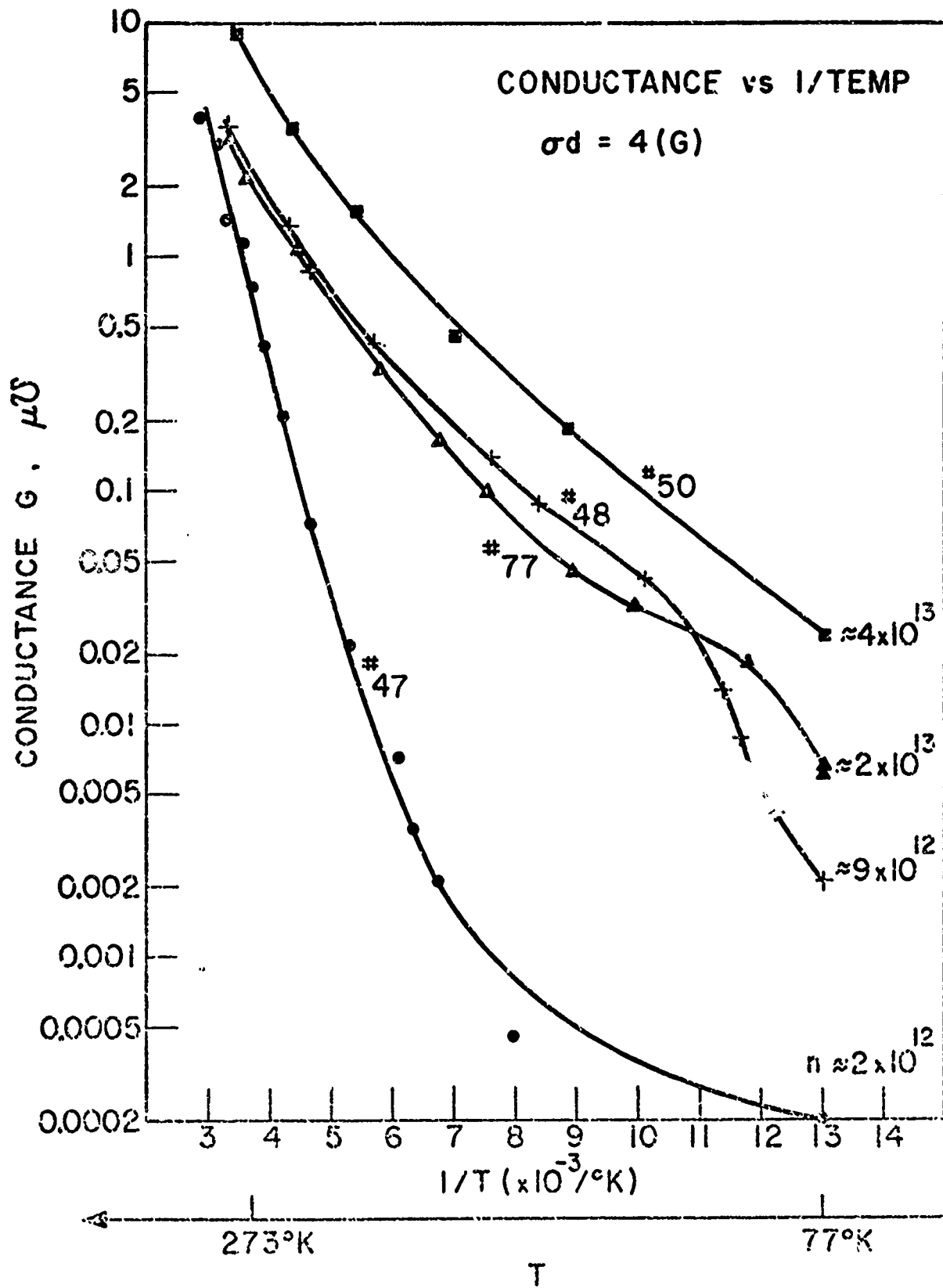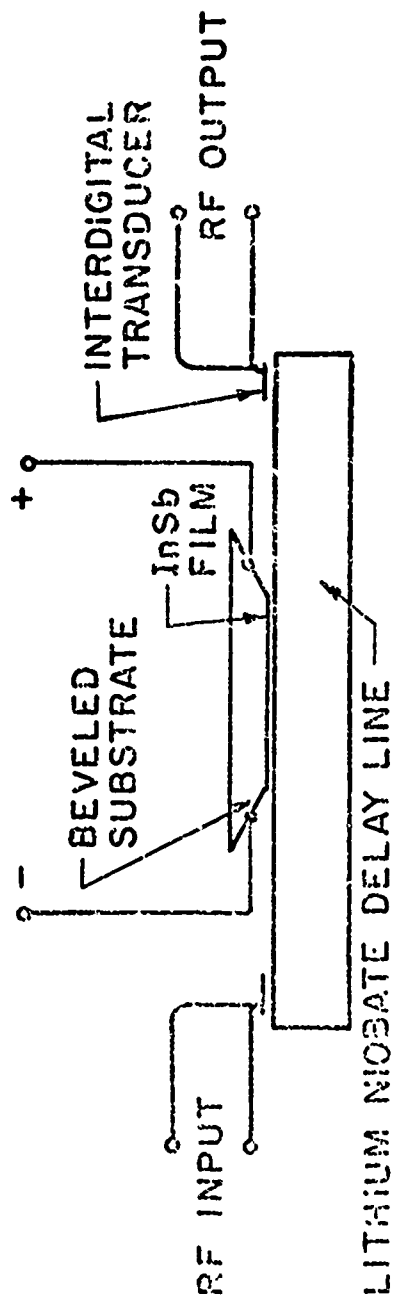
FIGURE 3

FIG. 4—Acoustic Surface Wave Amplifier.

achieve terminal gain in the amplifier, it is believed that electric fields of the order of 3 kV/cm will be required. During acoustic tests it has been demonstrated that fields of this magnitude can be sustained.

Amplifier tests have been carried out on several films, and acoustic gains of a few dB at 1000 J/cm have resulted in most cases. Since rigid substrates of 1mm thickness were used in all these tests, it is believed that some degree of mechanical contacting has always taken place when the film was brought close enough to obtain interaction. Similar results have been observed with silicon on rigid sapphire substrates in the past. We are planning to use a more flexible glass substrate 10 mils thick in the future.

Most of the present work is being directed toward the development of a monolithic acoustic amplifier. In short, this means using the piezoelectric delay medium as the InSb film substrate. Lithium niobate is a very good material for electrical coupling to surface waves and for this reason it is presently being used exclusively for surface wave acoustic amplifier tests in this laboratory. However, we have found that InSb cannot be directly deposited on lithium niobate when it is heated to 400°C in vacuum because of oxygen sublimation. We have found that one way of circumventing this problem is to coat the surface with ~ 200 Å of SiO. With this barrier layer in place a few oxide free films have been deposited. The electrical characteristics of the first of these samples was similar to those obtained using glass substrates. It should be pointed out, however, that most of the evaporation trials resulted in oxidized films, so that additional techniques for eliminating this problem are being considered. Contacts for this configuration can be made most easily by doping a narrow strip at each end of the film with indium.

In the near future we believe a good InSb film can be deposited on a lithium niobate delay line. This will give us the opportunity to compare the characteristics of this monolithic device with the theory and determine the feasibility of the configuration. Depending upon the behavior of the InSb - lithium niobate amplifier it will be decided whether to continue to use these materials or to consider other

semiconductor and/or delay line materials. Since the flash evaporation technique worked successfully with most of the III-V compounds,[7] it should be a minor effort to convert to the use of GaAs which has a much lower intrinsic density than InSb.

[7]E. K. Müller, J. Appl. Phys. 35, 580 (1964).

VI. SUBMILLIMETER WAVE GENERATOR

(H. Heffner, R. Meserve)

A. OBJECTIVE

The intent of this project was to utilize the differences in relaxation time of molecular energy levels to produce a population inversion in a flowing gas.

B. FINAL SUMMARY OF WORK

We have undertaken the theoretical study of the processes which control the buildup or decay of the populations of the vibrational levels of a molecule and studied the interrelations of these processes with each other. We chose to focus on the CO_2-N_2-He mixture because the current interest in these gases has generated an abundance of information in the literature.

In previous status reports we outlined the important relaxation processes which couple vibrational levels in the CO_2-N_2-He system, and on the basis of these processes, we constructed a set of rate equations. Given the starting conditions of the system and the changes of the parameters over time, the rate equations enable the determination of level populations at any instant of time, and consequently the gain of the system. The solution of these nonlinear equations was attained numerically by the use of Hamming's Predictor-Corrector method. As outlined in previous reports, we used our rate equations to model the gas transport laser of Tiffany, Targ, and Foster[1,2] and attained excellent agreement with their experimental data. We then extended our model to study the isentropic flow of the CO_2-N_2-He mixture through a high velocity nozzle. The nozzle serves to cool the

---

[1] W. B. Tiffany, R. Targ, and J. D. Foster, Appl. Phys. Letters 15, p. 91-3 (1969).

[2] W. B. Tiffany, private communication (1969).

kinetic temperature of the gas, and if the cooling is fast enough, can leave the CO_2 in an inverted state. The calculation for a mach 3 nozzle yielded both reasonable inversion and gain for the system. Our success with these two cases assured us that our model was fundamentally sound and that we could accurately predict the transient and stable level populations in a gas system.